Applied Surface Science 651 (2024) 159230

Contents lists available at ScienceDirect

Applied Surface Science

journal homepage: www.elsevier.com/locate/apsusc

Full Length Article

Design of an UV-C shielded biopolymer based on a poly(lactic acid)/quercetin/magnesium composite

Juan M. Casares-López [a,b], Margarita Hierro-Oliva [c,a,b], Verónica Luque-Agudo [d], M. Luisa González-Martín [a,b,c], Amparo M. Gallardo-Moreno [a,b,c,*]

[a] Departamento de Física Aplicada, Facultad de Ciencias, Universidad de Extremadura, Badajoz 06006, Spain
[b] Instituto Universitario de Investigación Biosanitaria de Extremadura (INUBE), Badajoz 06006, Spain
[c] Centro de Investigación Biomédica en Red: Bioingeniería, Biomateriales y Nanomedicina (CIBER-BBN), Badajoz 06006, Spain
[d] Departamento de Sistemas y Recursos Naturales, Escuela Técnica Superior de Ingeniería de Montes, Forestal y del Medio Natural, Universidad Politécnica de Madrid, Madrid 28040, Spain

ARTICLE INFO

Keywords:
Biopolymers
Poly(lactic acid)
Magnesium
Quercetin
UV-ageing

ABSTRACT

The use of biopolymers like poly(lactic acid) (PLA) doped with natural and harmless active agents in industrial, medical and food packaging applications is of great interest due to the multitude of property enhancements included. External factors, such as UV exposure, can accelerate the degradation process of these biomaterials and cause changes in structural and mechanical properties of medical or industrial devices. In this research, PLA-based composites with different degrees of crystallinity are fabricated using magnesium (Mg) particles and quercetin (Qr) as doping agents, providing new biomaterials with different responses against an UV-C radiation source. Physical surface changes are studied by atomic force microscopy (AFM), goniometry and scanning electron microscopy (SEM). Chemical modifications are evaluated by Fourier transform infrared spectroscopy (FTIR), X-ray photoelectron spectroscopy (XPS) and X-ray diffraction (XRD). Thermal response is studied by differential scanning calorimetry (DSC). PLA crystallinity is crucial in the polymer response to UV radiation. Under irradiation Mg particles cause a catalytic effect that enhances the degradation by hydrolysis of PLA chains. However, when Qr is present this effect is inhibited, making the Qr/Mg combination an ideal enrichment to protect the polymer from chemical photooxidation, while improving the surface mechanical properties of the new biocomposite.

1. Introduction

The physical and chemical properties of any material are decisive in its interaction with the environment and, in turn, any change in the surrounding medium can alter the chemical composition and the physical characteristics, such as surface free energy or elasticity. A comprehension of these changes is crucial for accurately predicting the behaviour of the material during its lifetime. In this context, one of the environmental factors that must be considered in the design of any material is ultraviolet light. This kind of radiation is widely used in different sterilization protocols for surgical materials, in food industry, in wastewater treatment and it is always present in materials exposed to the outside, as in the case of materials for agriculture, construction or automobile industry [1–9].

In all of those sectors, plastic-based materials are continuously selected for the implementation of different products. Plastics are ideal not only because of their advantages over other materials, such as metals, in terms of manufacturing versatility, but also due to the economic costs derived from their production. In particular, the considerable drop in the cost of producing polluting plastics has driven their use to the point of overexploiting their mass production for disposable packaging. Some of these polymers require hundreds of years to degrade completely. Therefore, this situation, together with the reduction of oil reserves, has encouraged significant research into the development of biopolymers obtained from renewable sources. The biodegradability properties of these materials make them particularly attractive in the biomedical industry (e.g. in controlled drug release systems) and in agro-food industry [10–14]. Current research is also focused on the development of suitable multifunctional composite materials, with a polymeric background, which combine all the advantages and overlap

* Corresponding author at: Departamento de Física Aplicada, Facultad de Ciencias, Universidad de Extremadura, Badajoz, 06006, Spain.
E-mail address: amparogm@unex.es (A.M. Gallardo-Moreno).

https://doi.org/10.1016/j.apsusc.2023.159230
Received 4 September 2023; Received in revised form 10 December 2023; Accepted 25 December 2023
Available online 27 December 2023

the possible drawbacks of the different materials involved [8,15–17].

Most of the currently available bioabsorbable materials are biopolymers based on poly(α-hydroxy acids), such as poly(lactic acid), poly (glycolic acid) and their copolymers. Specially, poly(lactic acid) (PLA) is one of the most employed materials for tissue engineering, drug delivery, 3D biomaterials printing, food active packaging, dentistry or modern agriculture [13,18–24]. This is due to its excellent biological compatibility, high transparency and mechanical strength, electronic or transportation properties, easy processability and availability, non-toxic nature or comparable mechanical properties to some other polymers [1,19,21,25]. It is also interesting to note that PLA degradation rate can be tuned with its crystallinity degree: crystalline samples are 3 to 4 times less permeable to oxygen and hydration water than amorphous ones [26]. Moreover, under physiological conditions, polymer degradation produces the division of the polymeric chains by hydrolysis releasing acid degradation products into the nearest environment [23,27]. This pH reduction, together with an elevated hydrophobicity [28] and, in some cases, an unfit hardness and an inappropriate degradation rate, makes it necessary to incorporate stabilizing fillers in the PLA matrix to overcome such drawbacks [29].

Magnesium is one of such fillers. In the biomedical field, this metallic element has demonstrated to prevent the acidification and inflammation of the human tissue surroundings, caused by polymer degradation. It also enhances the mechanical properties of PLA, improves the cell viability and increases its hydrophilicity and crystallinity [23,28,30–32]. Mg has also shown antibacterial properties against different types of bacteria, reducing the subsequent colonization and tissue infections [16,17,33–35]. However, magnesium also physiologically degrades and may also induce adverse effects due to its high corrosion rate, which promotes depolymerization and hydrolysis of ester groups in polymeric chains [23,28,36–40]. Other inorganic PLA fillers include magnesium oxide (MgO) [41], zinc oxide (ZnO) [18,19,42–45], titanium dioxide (TiO_2) [45,46] or hydroxyapatite (HA) [20,47]. In particular, Kim et al. [19] have proved that ZnO nanoparticles, besides their antibacterial activity, acted as a protective barrier against visible UV radiation, thus, proposing this biocomposite as a quite appropriate candidate for food packaging sector.

Evidently, not all the dopants employed to improve the properties of biopolymers like PLA need actually to be inorganic. In fact, another of the most cutting-edge lines of research is the incorporation of organic active fillers such as antibiotics, organic acids, or some vitamins [29]. Among all of them, flavonoids stand out as one of the most interesting options due to their distinctly active behaviour and extensive list of beneficial properties. Among the most important ones we can find their anti-inflammatory, antiviral, antiatherosclerosis, antiallergic, anticancer, antidiabetic, antioxidant, cardio-protective, anticarcinogenic and antibacterial effects [48–58].

Quercetin (Qr) is one of the most accepted flavonoids due to its discovered therapeutic applications to treat human diseases. It is part of the common intake of the human diet since it is present in fruits, leaves, vegetables, seeds, grains, and medicinal plants. One of the main characteristics of quercetin is its great chelation capacity with a large number of metal ions [48–52,59–64]. For instance, Marchionatti et al. [59] demonstrated that quercetin promoted calcium absorption by the intestine and decreased the bioavailability of metal ions such as nickel (Ni) or lead (Pb), which cause toxicity in human body [51,52]. Furthermore, an increase of biological activity of quercetin when chelated with suitable metal ion has been reported in several works. For instance, the coordination of Mg^{2+} with quercetin increased the bioactivity compared to that of the flavonoid alone, while at the same time improved the mechanical properties when embedded in a composite material [50–52,63]. Hence, there is no reason to miss the interesting opportunity to investigate the incorporation of such dopants into polymeric matrices. Just as Olewnik-Kruszkowska et al. [48] did when they reported antibacterial activity once quercetin was added to a PLA/PEG system. Or in the case of Di Cristo et al. [65], when they demonstrated that PLA nanofibers doped with quercetin showed antibacterial, antibiofilm and anti-inflammatory effects. Regarding food packaging applications, Sani et al. [66] checked the synergistic effect of adding zinc oxide, quercetin and natamycin as active fillers in a methylcellulose/chitosan blended system. They demonstrated the antibacterial activity and the antioxidant character of the composite after quercetin incorporation. Moreover, He et al. [67] designed an artificial periosteum based on a PLGA/MgO/quercetin composite, where suitable concentrations of quercetin coordinated with MgO showed osteogenic-angiogenic coupling effect, thus accelerating the repair of bone defects. Furthermore, quercetin is an organic dopant widely considered in food packaging biopolymer research due to the rising demand for natural antibacterial and antioxidant agents instead of chemical additives. Ezati et al. [68] evaluated the influence of loading quercetin into three different biopolymers for food active packaging purposes and proved that addition of quercetin into biopolymer matrices enhanced the UV-barrier properties and showed antioxidant and antibacterial behaviour against different bacterial strains.

Developing PLA-based composite materials that improves the properties and applicability of the polymer would ensure the material success in any of the sectors previously mentioned. However, as pointed out, we believe that environmental factors which may subsequently encounter the composite, such as an intense radiative disturbance by UV excitation, may not only alter biological structures but also modify its mechanical and surface structural properties. Indeed, the effect of UV-C irradiation on different biopolymers like poly(lactic acid) (PLA) [2–5,69–74], polyethylene terephthalate-glycol (PETG) [75], poly (ε-caprolactone) (PCL) [76], polyamide-6 [77], poly(2-ethyl-2-oxazoline) [78] or poly(butylene adipate-co-terephthalate) (PBAT) [79] is of high interest. For instance, Amza et al. [75] analyzed the changes in mechanical properties of 3D-printed elements based on PLA and PETG after 24 h of UV-C exposure. They registered a decrease of about 2 and 6 % in Young's modulus values of PLA and PTEG, respectively, after irradiation. Furthermore, Czechowski et al. [3] investigated the influence of nanoadditives in the UV ageing process of biopolymers by adding graphene nanopowder into printed PLA matrix. They recorded a loss of approximately 25 % in Young's Modulus of PLA after UV-C exposure. Likewise, Wang et al. [79] even proposed a degradation mechanism based in a series of Norrish chemical reactions, in order to clarify the photolysis process of PLA, after exploring the influence of UV-C light in the polymer matrix modifications of a novel and multifunctional PLA/PBAT blended system.

On this basis, this research will fabricate PLA-based composite materials, using Mg and quercetin, which will exhibit different chemical and physical response to an intense UV-C radiation source, defining specific conditions for self-protection. Composites with a different PLA crystallinity degree will be prepared by solvent-casting method and its mechanical and chemical response to prolonged UV-C light exposure will be tested. Physical surface changes will be addressed through Atomic Force Microscopy, Goniometry, Scanning Electron Microscopy and Differential Scanning Calorimetry. Chemical modifications will be evaluated with Fourier-Transform Infrared Spectroscopy, X-ray Photoelectron Spectroscopy and X-Ray Diffraction. The novelty of this research lies in the fact of including a natural substance such as Qr in the manufacture of the well-known PLA/Mg biocomposite to protect it from the degradative effects associated to UV exposure. The primary application is essentially found in the biomedical and food packaging fields where UV-C is used in sterilization processes of biomaterials

2. Material and methods

2.1. Sample preparation

2.1.1. Sample materials and chemical reagents

Amorphous poly(lactic acid) particles (PDL04, copolymer of DL-lactide with an inherent viscosity midpoint of 0.4 dL g^{-1}) were

purchased from PURASORB© (Corbion, Amsterdam, the Netherlands) and were used as received. Crystalline PLA (PLA2003D, with a D-isomer content of 4.25 %) particles were purchased from NatureWorks L.L.C. (Blair, NE, USA) and were used as received. PLA films were manufactured onto glass disks (25 mm diameter and 2 mm thickness), purchased from Garvaglass S.L.L. (Santa Perpetua de Mogoda, Barcelona, Spain). Before use, glass disks were immersed in chromic acid for 15 min and the rinsed with deionized water. They were kept in a dessicator until use. Chloroform (Sigma-Aldrich, MO, USA, purity > 99.5 %) and ethanol absolute pure (PanReac AppliChem, Barcelona, Spain, purity > 99.5 %) were used to dissolve PLA and quercetin powder (Sigma-Aldrich, China, purity > 95 %), respectively. For preparation of films with Mg, magnesium particles (≤50 μm), purchased from Nitroparis (Castellón, Spain), were used.

2.1.2. Films preparation

PLA films were fabricated following the solvent-casting protocol described by Luque-Agudo et al. [80,81] in previous works. Due to the difference in density and viscosity of amorphous and crystalline PLA, each one was dissolved in chloroform in different concentrations. For amorphous PLA films, the ratio with respect to the solvent was 20 % (w/v), and 5 % (w/v) in the case of crystalline ones. Therefore, the resulting solutions would encounter similar density and viscosity values. Also, with the aim of comparing results between amorphous and crystalline PLA, both types of films were doped with the same quantity of active fillers. So, magnesium and quercetin quantities were calculated based on the percentage by weight relative to crystalline PLA.

Amorphous and crystalline PLA granules were dissolved in chloroform with a magnetic rotator at room temperature. Then, the PLA solutions were divided in four and those corresponding to quercetin, Mg and quercetin/Mg were mixed with the specific dopants using a rotator stirrer (JP Selecta, Barcelona, Spain) for 30 min. In the case of PLA/quercetin condition, PLA/chloroform and quercetin/ethanol solutions were mixed in suitable proportion (27 % v/v of quercetin/ethanol mixture in PLA/chloroform solution, which leads to the 13.5 % w/w concentration of quercetin in PLA film). For PLA/Mg condition, 10 % w/w of Mg was added to the PLA/chloroform solution. For PLA/quercetin/Mg condition, PLA/chloroform and quercetin/ethanol solutions were mixed first and Mg particles were added later. Then, a volume of each of the four types of final conditions (0.51 mL) was deposited onto glass disks and were left to dry first at room temperature for 4 h and later in an oven at 65 °C for 48 h to completely remove any remaining solvent [81]. Thus, the thickness of the films was controlled by depositing the same dissolution volume onto the glass disks. And, since the evaporation conditions of the solvent were also controlled, the mean thickness would be quite similar among the samples. Moreover, in previous works [81], the thickness of PLA films was controlled by making cross sections and measuring them by Scanning Electron Microscopy (SEM, FEI Company, Quanta 3D FEG, Hillsboro, OR, USA). Also, in those cases of difficulty to cut the PLA films, like in amorphous ones, the thickness was controlled by measuring with a confocal optical profilometer (LEICA DCM8, Germany). With this equipment, the thickness can be measured through the films due to their transparency. So, comparing the distance between the focus at the top of the glass substrate and the focus at the top of the PLA film, the values obtained for the thickness agreed considerably with those obtained previously by SEM.

2.2. UV light ageing procedure

PLA films doped with quercetin, Mg and their mixture were exposed to a UV-C source for 23 h. This period was sufficient to guarantee an optimal sterilization process and a more than sufficient representation of prolonged exposure to natural UV radiation [1,6,9,75,82,83]. A high-pressure mercury lamp, working at a wavelength of 254 nm and at a mean intensity of 2.09 ± 0.05 mW cm^{-2}, was used as the UV light source, kindly provided by Philips (Philips Iberica, Spain). The disks were positioned at 100 mm from the light source and centred, receiving a mean dose of 169.8 ± 3.7 J cm^{-2} measured by a cosine-corrected sensor connected to a dosimeter UV-MAT (OPSYTEC Dr. Gröbel GmbH-Germany). The temperature at the sample level inside the chamber was 25 °C. Air circulation was maintained in order to remove the ozone originated in the oxygen UV irradiation. The experimental procedure of accelerated ageing process was assessed following the ISO 4892-3:2016 standard [84], which provided a guidance on how to proceed with data in accelerated UV irradiation tests. Henceforth, the nomenclature to be used to describe each crystallinity and doping condition will be PLAx/Y/Z, where "x" can be "a" for amorphous films or "c" for crystalline ones and "Y" and "Z" refer to the possible presence of quercetin (Qr) and/or Mg particles, respectively. Also, when films were exposed to UV-C light, it will be added a "+UV" to the condition name.

2.3. Surface structure characterization

Morphology of surface of PLA films cast on glass disks was evaluated by using an atomic force microscope (AFM) (Agilent 5500, Agilent Technologies, California, CA, USA) operating at room temperature in contact mode. Rectangular cantilevers (FMV-PT, Bruker, Billerica, MA, USA) were used with a natural frequency of 75 kHz and a spring constant of 2.8 N m^{-1}. Four-sided pyramidal tip radius had a nominal curvature radius of 25 nm and a half-opening angle of 22.5°. Images were taken for two scanning lengths (10 × 10 μm^2 and 2 × 2 μm^2) and in each scanning area, topographical, deflection and friction images were acquired. Experiments were performed in triplicate, studying three different films for each condition and three different areas for each film before and after UV exposure. The most representative images from the three areas of the triplicate for each different condition will be shown with their corresponding height scales. Not only the morphology but also the topography was evaluated through the acquisition of mean surface roughness (Sa) parameter by free SPM software Gwyddion (v. 2.64, Czech Metrology Institute). Moreover, AFM tip morphology was characterized with SEM in order to verify its working dimensions with those provided by the manufacturer.

2.4. Mechanical properties

The effect of UV-C irradiation on mechanical properties of PLA films, with two degrees of crystallinity and doped with different active compounds, was evaluated by the AFM introduced in Section 2.3. Also, the same cantilevers used for topography measurements were employed for acquisition of Young's modulus values through force-distance (*F-d*) curves. Regarding previous technical works from AFM tip manufacturer (Bruker, Billerica, MA, USA), the spring constant value used in this work is suitable for samples with Young's modulus of MPa-GPa order [85]. This is the range of Young's modulus values expected and widely tabulated for PLA films [2–5,69–74].

Prior to force spectroscopy experiments, AFM photodiode sensitivity, or just deflection sensitivity, was calibrated by measuring force-distance curves on a 316 LVM austenitic stainless-steel disk (Surgival SL, Valencia, Spain), which was assumed to be non-deformable. The values obtained for deflection sensitivity depend on the working tip properties, the medium where measurement is performed or the laser position on the AFM cantilever, which modifies its optical path. Hence, the photodiode sensitivity value was maintained for all the force-distance curves obtained in order to be able to correlate the results between different samples.

In a force vs. distance (*F-d*) experiment, AFM cantilever approaches sample surface by modifying piezoelectric height (*Z*) (Fig. 1). When the tip feels the interaction with the surface (mostly long-range forces such as Van der Waals or electrostatic forces) the cantilever starts to bend downwards until well-known *jump-to-contact* takes place. If cantilever keeps decreasing its piezoelectric *Z*-positioning, it bends upwards, and the tip starts to indent the surface and cause a sample deformation.

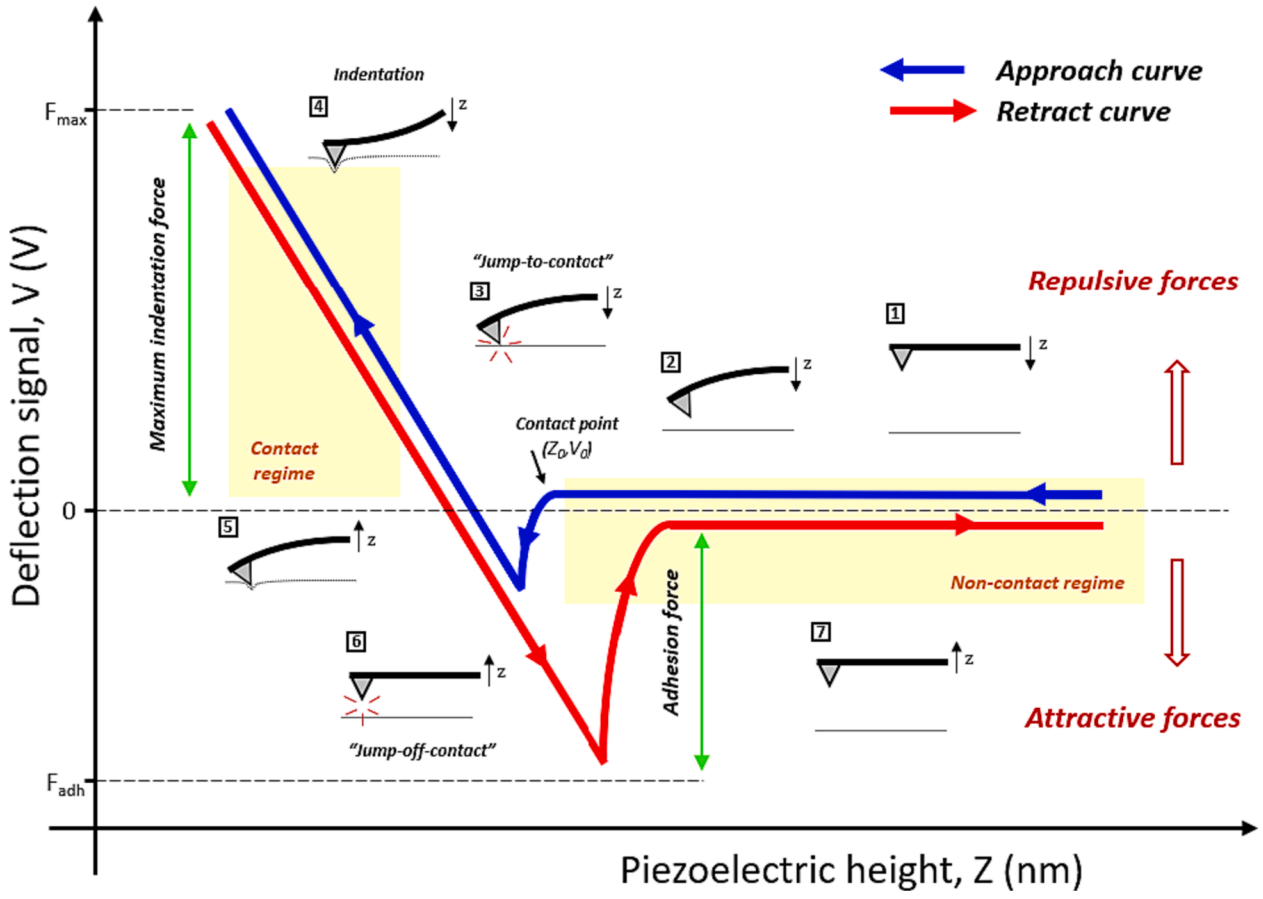

Fig. 1. Indentation cycle where the tip approaches to the sample surface as cantilever starts to bend until "jump-to-contact" occurs. Then, the piezoelectric height keeps decreasing and the tip starts to indent the surface producing a sample deformation. After indentation, piezoelectric goes back until "jump-off-contact" takes place and tip separates from the surface. This cycle is recorded in approach-retract curves across the surface to obtain the Young's modulus values from the proper fitting.

When the cantilever goes upwards in *Z*-direction after indentation, it stretches the surface until *jump-off-contact* occurs (deeply related to adhesion and capillarity forces) [86]. This cycle is repeated across the surface to obtain statistically consistent Young's modulus values. Between one indentation and other, it should be considered the hysteresis suffered from the approach/retract movement, which is a consequence of viscoelastic response of the sample. Thus, we decided to wait 10 s between one measurement and the next one [86]. Also, similar to the topography measurement procedure, indentations were performed on scanning areas of $10 \times 10\ \mu m^2$ and $2 \times 2\ \mu m^2$ (with no scale overlapping in the same zone), with a surface density of 256 measurements per image.

Since cantilever deflections are detected by the AFM photodiode, force output values are expressed in voltage terms (*V*). However, the deflection sensitivity (*DS*) measured, and the spring constant k_c (previously calibrated by thermal noise method) allow the conversion of voltage values into force units by Hooke's law application. Also, piezoelectric height and cantilever deflection were scaled to the contact point, which is the (Z_0, V_0) point at which AFM tip first notices the interaction with the sample surface. With this information, *F-d* curves were transformed into force–deformation (*F-*δ_S) curves and then, they can be fitted by using different models. Pyramidal tips have some relevant advantages when mapping the local viscoelastic properties of soft samples [87]. Thus, the solution for a regular four-sided pyramidal tip proposed by Rico et al. [88] based on Bilodeau theory [89] has been chosen for obtaining Young's modulus values in our work:

$$F(\delta_s) = \frac{\tan\alpha}{\sqrt{2}} E_R \delta_s^2 \tag{1}$$

Where $F(\delta_S)$ is the force exerted on the sample by the tip, δ_S is the sample deformation, α is the half-opening angle of the tip pyramidal geometry (taken as 22.5°) and E_R is the reduced Young's modulus, which is related with Young's modulus of the surface sample, E_S, as shown in Equation (2).

$$\frac{1}{E_R} = \frac{1-\nu_s^2}{E_s} + \frac{1-\nu_{tip}^2}{E_{tip}} \tag{2}$$

Where ν_S is the Poisson ratio of the sample and ν_{tip} and E_{tip} are the Poisson ratio and Young's modulus of the AFM tip. It is important to point out that E_S refers to the Young's modulus of the surface of the samples studied, which differs from the *E* values from the bulk. However, this work evaluates the surface response of doped PLA films against UV irradiation, so bulk properties will not be considered, although they are clearly related. Contact point detection has been carried out by implementing the algorithm in R software (R Core Team (2022). R: A language and environment for statistical computing. R Foundation for Statistical Computing, Vienna, Austria) published by Benítez et al. [90]. Moreover, Equation (1) has been linearised to fit the experimental results. In particular, once E_R was obtained, E_S was calculated from Equation (2), considering the approximation that AFM tip has a remarkably higher modulus than the sample. Then, if $E_{tip} \gg E_S$, Equation (2) becomes:

$$E_R \approx \frac{E_s}{1-\nu_s^2} \quad (3)$$

And Equation (1) can be written as:

$$F(\delta_s) = \frac{\tan\alpha}{\sqrt{2}} \frac{E_s}{1-\nu_s^2}\delta_s^2 \quad (4)$$

Where ν_S was taken as 0.4 for all the conditions. Based on previous works, such as Rezgui et al. [91], Farah et al. [92] or Mirkhalaf et al. [93], PLA Poisson ratio ranges from 0.36 to 0.42. Also, Cifuentes et al. [94], Li et al. [95] and Mozafari et al. [96] worked with Poisson ratio values within the previous range when evaluating the mechanical properties of PLA and magnesium composites.

2.5. Contact angle and surface free energy

Contact angle measurements were performed at room temperature under ambient conditions with a Krüss goniometer (Krüss, Hamburg, Germany) and the Drop Shape Analyzer software (Version 1.12.2.06901, Krüss GmbH, Hamburg, Germany), based on the sessile drop method. In both before and after UV experiments, three liquids with different polarities were used: deionized water (Milli-Q Integral 5 System, Merck, Darmstadt, Germany), ethylene glycol (Fluka, Thermo Fisher Scientific, Waltham, MA, USA) and diiodomethane (Fluka, Thermo Fisher Scientific, Waltham, MA, USA) whose surface tension components are well-known [97]. At least, five drops of each liquid were deposited on each sample corresponding to the triplicate of each condition and drops of 5 μL of deionized water, 10 μL of ethylene glycol and 2 μL of diiodomethane were placed at different positions on the surface of the samples [98]. Drops were photographed at 15 s after their complete deposition to measure the static contact angles. This time was enough to guarantee the equilibrium contact angle between the liquid and the surface. Thus, the surface free energy components of the films were calculated according to the approach of van Oss et al. [99–102] and their uncertainties were obtained by error propagation methodology. Contact angle and surface free energy values will be expressed as mean ± standard deviation.

2.6. Fourier-transform infrared spectroscopy

FTIR analysis of non-irradiated and irradiated samples was carried out by a VERTEX 70 spectrophotometer (Bruker, Billerica, Massachusetts, USA) with a Praying Mantis cell (Harrick Scientific, Pleasantville, NY, USA). The working mode was Diffuse Reflectance Infrared Fourier Transform Spectroscopy (DRIFTS), where irradiation does not cross the whole sample, but it is diffusely reflected by the outermost surface layers of just a few microns depth, and then recorded by a Deuterated Lanthanum α Alanine doped TriGlycine Sulphate (DLaTGS) detector (Bruker, Billerica, Massachusetts, USA). The spectral resolution was 0.4 cm^{-1} in the 4000–400 cm^{-1} spectral range studied.

2.7. Differential scanning calorimetry

DSC analysis was performed on amorphous and crystalline doped PLA films before and after UV-C irradiation with a 214 POLYMA DSC (NETZSCH GmbH, Selb, Germany). The measurements were carried out with a resolution of 0.1 μW and an enthalpy precision of ± 0.05 to ± 0.2 %. At least 3 mg from each film were obtained to measure between aluminium platelets. The total flux was 100 mL min^{-1} and the heating was performed from 0 to 200 °C or from −20 to 200 °C with a ramp of 10 °C min^{-1}. The equipment calibration was achieved by control samples from NETZSCH: 2100401 (In), 22032501 (Sn), 130720 (Bi), MKCQ7668 (Zn), 20033101 (CsCl). Glass transition temperature (T_g), melting temperature (T_m) and % of crystallinity (X_C) were obtained through DSC curves by *Proteus*® software (NETZSCH, Germany). Crystallinity calculation was done by linear integration considering a melting enthalpy, ΔH_m^0, of 93 J g^{-1} for 100 % crystalline PLA [103,104].

2.8. X-ray photoelectron spectroscopy

XPS evaluation was achieved by the analysis and quantification of spectra obtained from a XPS system FlexPS-ARPES-E SPECS spectrometer (Berlin, Germany). A monochromatic Al Kα (1486.68 eV) X-ray source was employed at a voltage of 15 kV and a current of 6.6 mA. Source was located at 56.5° of inclination respect to the normal of each sample measured. Stabilization vacuum was reached at $5 \cdot 10^{-10}$ mbar and working vacuum at $1.6 \cdot 10^{-9}$ mbar, by the Flood Gun application. Survey spectra were captured using a pass energy of 100 eV. High-resolution peak spectra were obtained with a pass energy of 30 eV. Spectral energy resolution was fixed at 0.9 % of pass energy. The high-resolution XPS spectra were background subtracted using the Shirley method and deconvoluted using a mixed Gaussian/Lorentzian peak shape with the XPSPeak software (version 4.1).

2.9. X-ray diffraction

XRD analyses were conducted by a D8 ADVANCE diffractometer (Bruker, Germany), using a monochromatic Cu $K\alpha_1$ ($\lambda = 1.5406$ Å) from Ge 111 monochromator. The samples were scanned from 2θ of 10 - 60° with a 0.02° step size and a source at 30 kV and 40 mA. The analysis was performed on PLA control samples before UV-C irradiation by duplicate and in three different zones to obtain consistent statistics and to check the differences between amorphous and crystalline PLA's X-Ray diffractograms.

2.10. Statistical analyses

Statistical design was assessed by the implementation of factors representing the different variables involved in each of the experiments. Statistical analysis was carried out with R software (R Core Team (2022). R: A language and environment for statistical computing. R Foundation for Statistical Computing, Vienna, Austria). After checking the presence of normality in the response variable and a comparable homoscedasticity between different groups, data were analyzed using one-way analysis of variance (ANOVA). Consequently, post-hoc Tukey's multiple comparison test was applied. Otherwise, Kruskal-Wallis test was carried out. Specifically, in the case of an overall analysis of whole data such as the seek of some interaction between PLA crystallinity, dopant presence or UV-C irradiation factors, full-factorial ANOVA test was performed. All analyses were considered at a significance level of $p < 0.05$ and the main results will be presented as mean ± standard deviation.

3. Results

3.1. Qualitative surface characterization

3.1.1. Amorphous PLA films under UV-C irradiation

Qualitative changes in amorphous PLA films are shown in Fig. 2. Before irradiation, PLA control films remained practically transparent with a glossy finish after deposition onto glass disks. When quercetin was added, the film acquired the characteristic yellowish colour from this natural compound. After magnesium incorporation to the PLA dissolution, the inorganic particles could be appreciated within the transparent polymer matrix following a random diffusion pattern. Likewise, when the dopant mixture was included, the film obtained a new dark-brownish yellow. In all cases, a kind of shiny varnishing can be perceived in the outermost layers of amorphous films.

After UV-C exposure, PLA films aspect was considerably modified in some cases. Spherical bubble-shaped structures appeared in the absent of any dopant and so, surface topography was visually altered. Also,

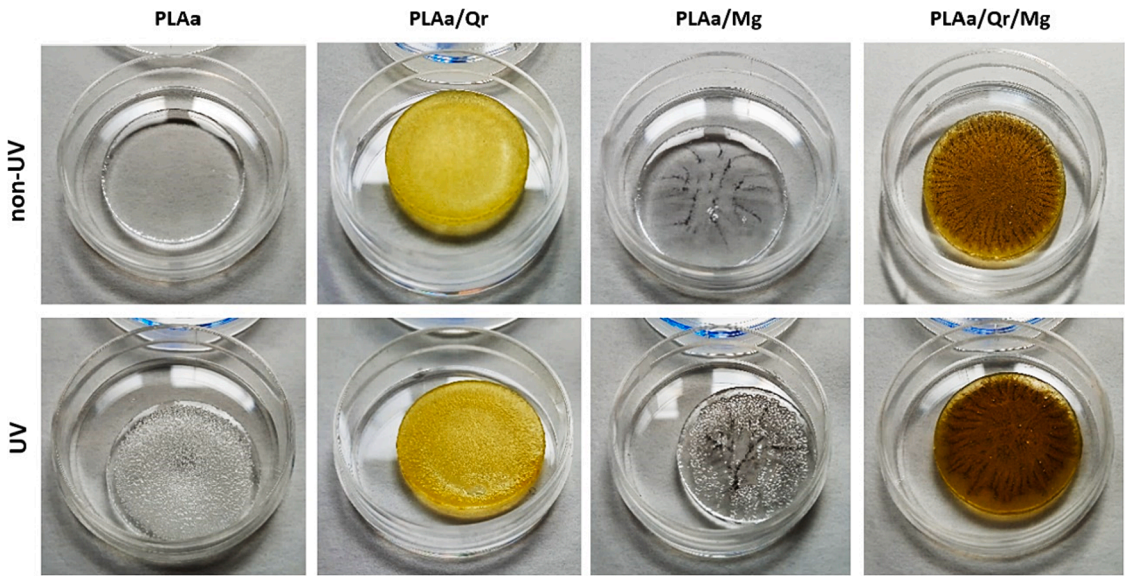

Fig. 2. Qualitative changes in amorphous PLA control films (PLAa), with quercetin (PLAa/Qr), and magnesium (PLAa/Mg) and with quercetin and magnesium (PLAa/Qr/Mg) (from left to right) before (non-UV) and after (UV) UV-C irradiation (from top to bottom).

when magnesium particles were present in the PLA matrix, these structures appeared but in a lower quantity. Nevertheless, when quercetin was added as a dopant, either alone or mixed with Mg particles, the appearance of spherical structures was completely eradicated. It was only appreciated a slight change in the shade of yellow when UV-C light was applied.

3.1.2. *Crystalline PLA films under UV-C irradiation*

In the case of crystalline PLA films (Fig. 3), control films acquired a more translucent and wavy aspect than amorphous ones after their deposition onto glass disks. Similarly, when magnesium was incorporated to the crystalline PLA matrix, random diffusion paths could be recognized. Once quercetin was integrated, the resulting surface acquired a uniform yellowish matt colour when added alone and turned to brown when magnesium was coordinated. In both cases, a higher degree of crystallinity in PLA produced a bumpy rugged texture when quercetin or quercetin/magnesium mixture were present.

Conversely to amorphous PLA, when UV-C treatment was performed in crystalline PLA films, bubbles were not appreciated in any case.

3.2. *AFM morphology examination*

AFM topographic images were obtained to evaluate the influence of quercetin and/or magnesium presence in PLA matrix before and after UV-C irradiation.

In the case of amorphous PLA samples (Fig. 4), there is no significant influence of magnesium, quercetin, or magnesium/quercetin mixture presence in the surface texture. Amorphous PLA films maintain mean surface heights values around a few nanometres, regardless the dopant incorporation. However, after UV-C exposition, surface heights increase to several tens of nanometres. Similarly, dopant effect is not detectable after irradiation. Hence, amorphous PLA morphology is characterized by a nanometrical flatness and a clear susceptibility to UV-C light. In this case, large-scale differences in surface texture as a consequence of UV-C

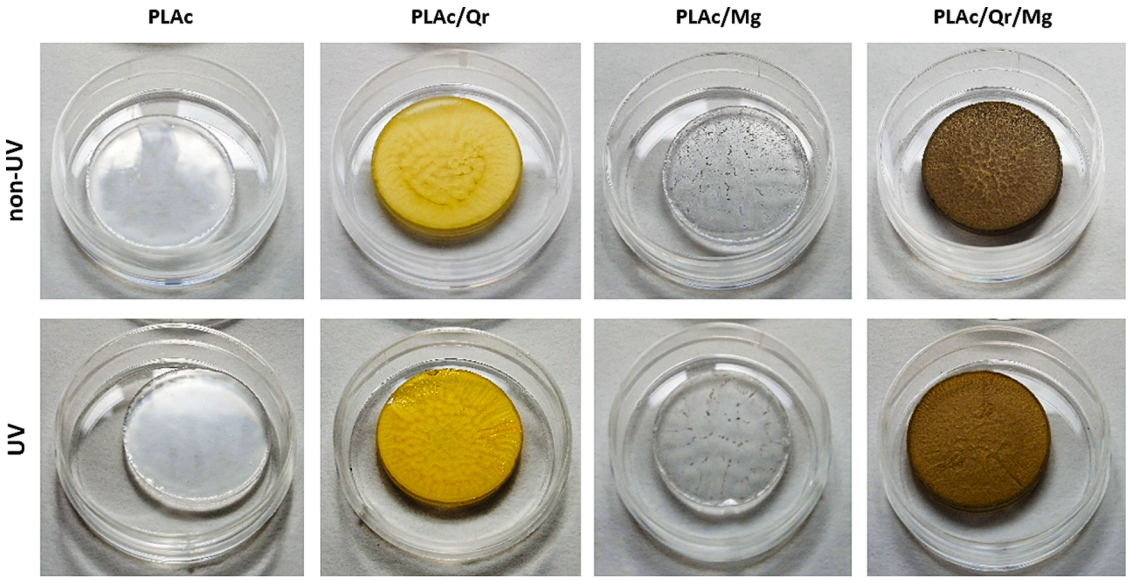

Fig. 3. Qualitative changes in crystalline PLA control films (PLAc), with quercetin (PLAc/Qr), and magnesium (PLAc/Mg) and with quercetin and magnesium (PLAc/Qr/Mg) (from left to right) before (non-UV) and after (UV) UV-C irradiation (from top to bottom).

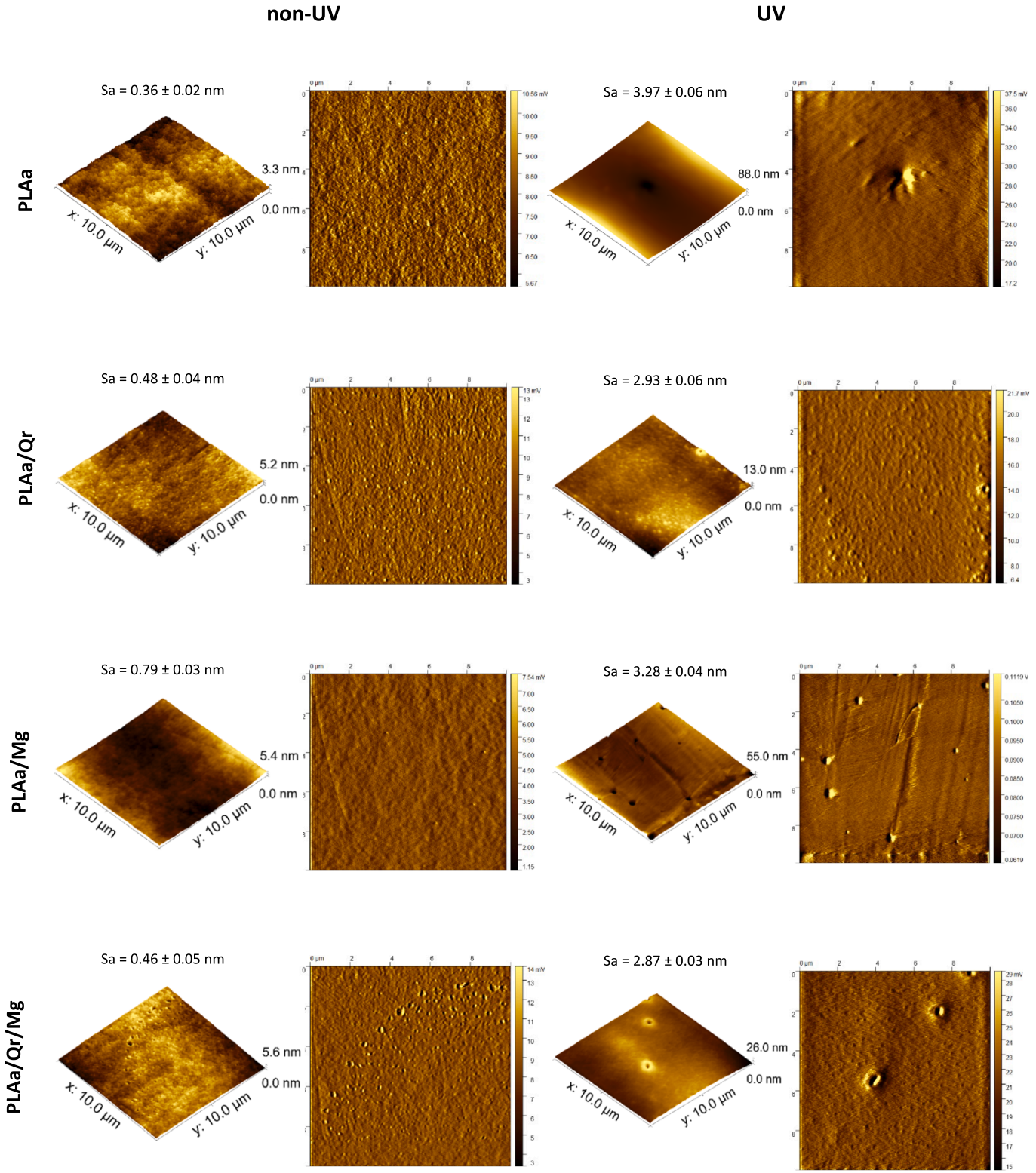

Fig. 4. 3D-AFM topography images and 2D-deflection images of amorphous PLA films in control, quercetin, magnesium and quercetin/magnesium conditions (from down to bottom), before and after UV-C irradiation (from left to right). All images have only been processed with a flattening filter in order to maintain a higher degree of rawness in data. Mean surface roughness, Sa, has been obtained for each condition.

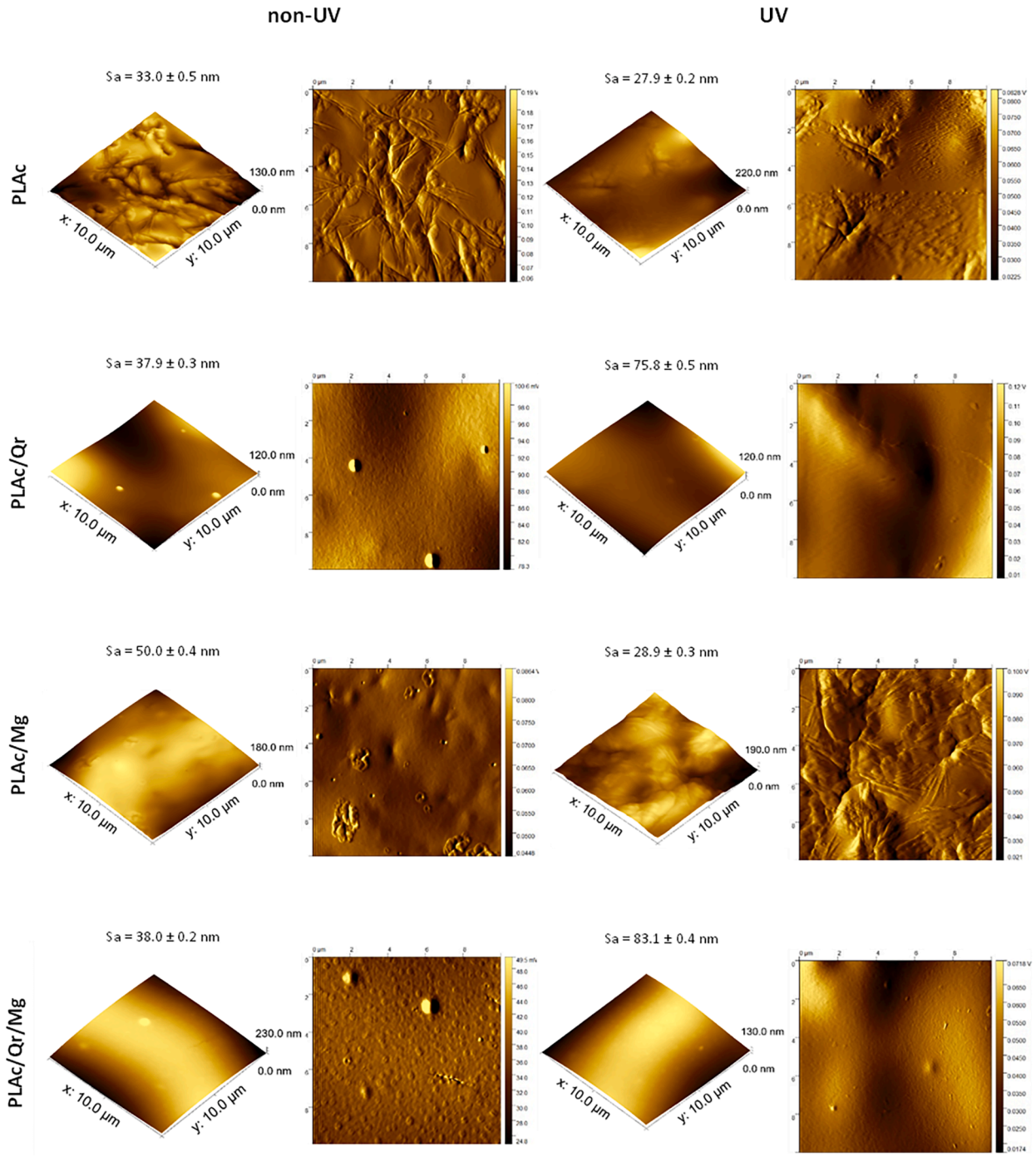

Fig. 5. 3D-AFM topography images and 2D-deflection images of crystalline PLA films in control, quercetin, magnesium, and quercetin/magnesium conditions (from down to bottom), before and after UV-C irradiation (from left to right). All images have only been processed with a flattening filter in order to maintain a higher degree of rawness in data. Mean surface roughness, Sa, has been obtained for each condition.

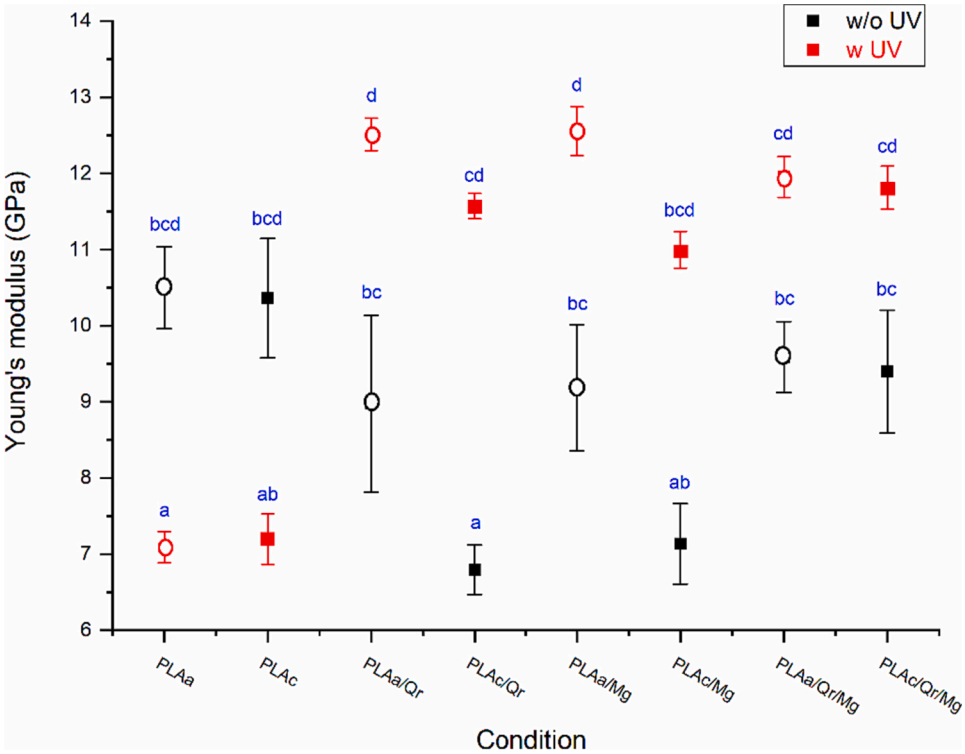

Fig. 6. Young's modulus representation for amorphous and crystalline PLA films in control, quercetin, magnesium and quercetin/magnesium conditions, with (red) and without (black) UV-C irradiation. In the graphic, "PLAa" stands for amorphous PLA films and "PLAc" for crystalline films. Statistical results (blue) from post-hoc Tukey's multiple comparison test are attached to each corresponding mean ± s.d. value, where dopant presence, PLA crystallinity degree and UV exposition were taken as factors. (For interpretation of the references to color in this figure legend, the reader is referred to the web version of this article.)

exposure, such as bubbles appearance (Section 3.1), are not discernible to the AFM. Nonetheless, amorphous PLA sensitivity to UV-C light reaches even micro-nanometrical scales where the AFM can perceive the possible surface alterations.

In contrast, crystalline PLA surface (Fig. 5) is characterized by a wavy texture with some ribbed structures. These features can only be appreciated in control and magnesium conditions. When quercetin was added, the surface texture became softer. In all cases, dopant presence does not influence the mean surface heights before and after irradiation. Unlike in amorphous PLA, UV-C light does not clearly increase surface heights values in crystalline PLA films. Indeed, they keep in the range of 100–200 nm. Thus, crystalline PLA films acquire a rougher surface texture from manufacture than amorphous ones.

3.3. AFM measurements of Young's modulus values

Prior to analyse the effect of active fillers and UV-light in PLA films, a statistical study was applied to examine the dissimilarities in Young's modulus values from different scanning areas (10×10 μm^2 and 2×2 μm^2). As expected, Young's modulus is not a scale-dependent magnitude, so no statistically variation was found between values from one scale-length and other. Then, data from both scanning areas were included in Young's modulus analysis for all the dopant, PLA crystallinity degree and ultraviolet ageing conditions.

Before UV-C irradiation, there is no remarkable difference in Young's modulus between amorphous and crystalline PLA control samples (Fig. 6). In the case of amorphous films, there is a slight drop in average data after quercetin, magnesium and quercetin/magnesium addition; but differences are not significant compared to the control condition. Nonetheless, in the case of crystalline films, there is a notable reduction of Young's modulus when quercetin and magnesium were added separately. In addition, if both compounds are added together, the reduction was modulated. Therefore, the interaction of quercetin with magnesium particles inside the pristine crystalline PLA matrix produced a positive effect that maintains the Young's modulus values at the level of control conditions.

After UV-C irradiation, a statistically significant loss of Young's modulus values for control PLA samples (both amorphous and crystalline) can be observed. Indeed, it can be quantitatively obtained a reduction of about 32.4 % for control amorphous films and 30.5 % for control crystalline ones. Contrary to what was obtained before irradiation, the observed effect of dopant presence into polymeric matrix is now modified by the UV-C excitation. Indeed, the embedding of quercetin and/or magnesium into PLA films avoid the remarkable drop in Young's modulus suffered by control samples after ultraviolet exposure. Moreover, in this situation, the dopant effect even increases the elastic modulus values for control amorphous and crystalline films. Regarding the effect of PLA crystallinity degree, there is a clear difference between amorphous and crystalline PLA when quercetin or magnesium were included separately. In fact, the drop in Young's modulus respect to the control is more obvious in crystalline films before UV irradiation. After UV irradiation, the increase in elastic modulus values is higher for amorphous samples. However, data from amorphous and crystalline tend to match when quercetin and magnesium are added together, either before or after irradiation. Lastly, it is also important to stand out the homogenisation of the Young's modulus values after ultraviolet exposure reducing the standard deviations.

3.4. Contact angle measurements and surface free energy determination

Water contact angle values for control PLA films (Fig. 7) confirm the hydrophobic character of this biopolymer due to its specific groups in its chemical structure, which originate strong intermolecular hydrogen bonds within polymeric chains [105]. Moreover, there is no significant difference in θ_w values between amorphous and crystalline PLA films with different dopant conditions. Therefore, there is no dependence of

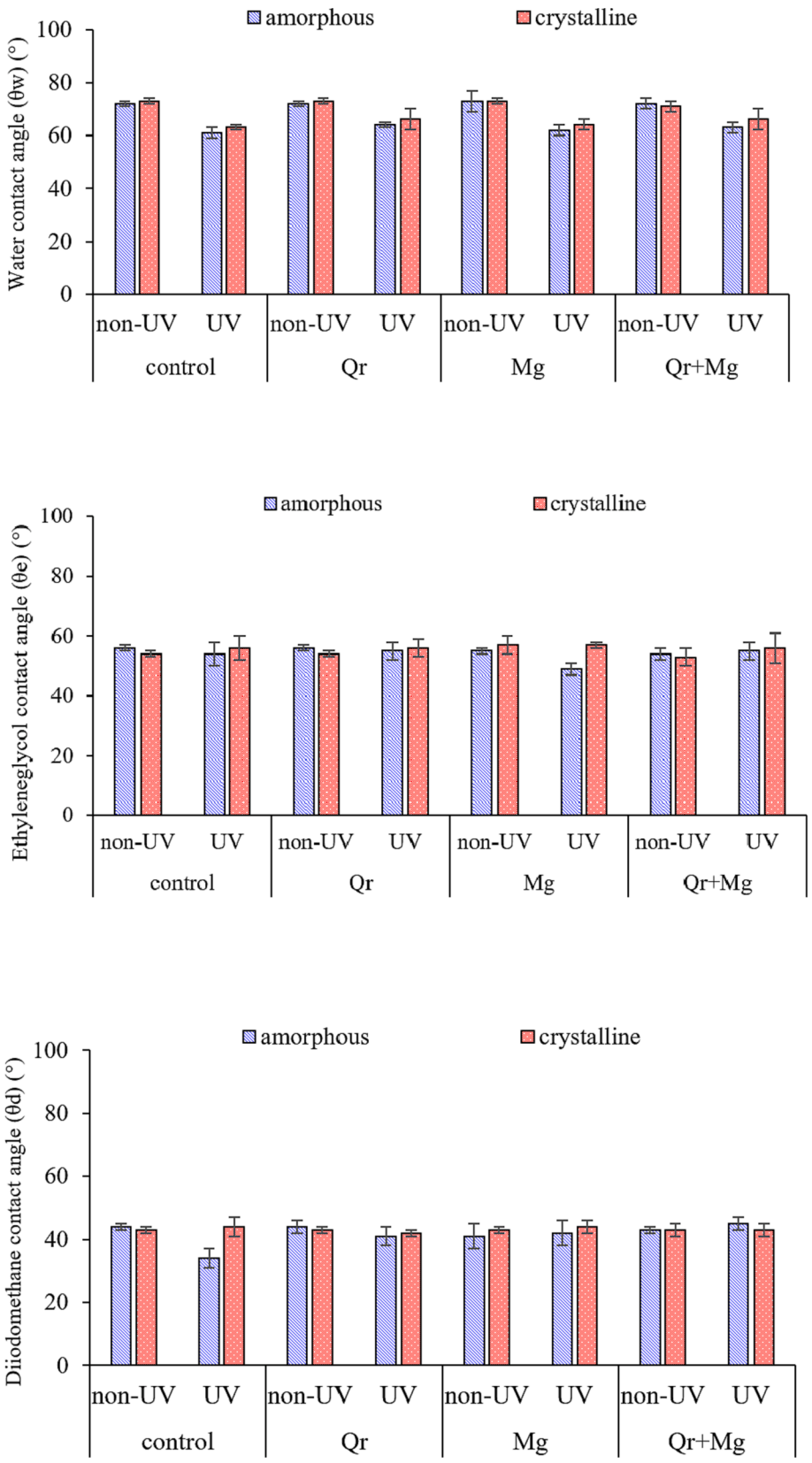

Fig. 7. Contact angle values for amorphous and crystalline PLA films in control, quercetin, magnesium and quercetin/magnesium conditions, non-irradiated and irradiated with UV-C light. Angles were obtained with three different liquids: deionized water (top), ethylene glycol (middle) and diiodomethane (bottom).

Table 1
Surface Free Energy values for amorphous and crystalline PLA films in control, quercetin, magnesium and quercetin/magnesium conditions, non-irradiated and irradiated with UV-C light. Different components of the surface free energy were obtained through the van Oss approximation: Lifshitz-van der Waals, γ^{LW}, acid-base, γ^{A-B}, electron-acceptor parameter, γ^{+}, electron-donor parameter, γ^{-} and surface free energy of solid, γ^{S}. In the table, "PLAa" stands for amorphous PLA films and "PLAc" for crystalline films.

UV-C irradiation	Sample	Surface Free Energy components (van Oss approximation)				
		γ^{LW} [mJ m^{-2}]	γ^{A-B} [mJ m^{-2}]	γ^{+} [mJ m^{-2}]	γ^{-} [mJ m^{-2}]	γ_S [mJ m^{-2}]
Non-irradiated	PLAc	32.8 ± 0.6	2.3 ± 0.6	0.09 ± 0.04	13.8 ± 1.2	35.1 ± 1.1
	PLAc/Qr	32.8 ± 0.6	2.3 ± 0.6	0.09 ± 0.04	13.8 ± 1.2	35.1 ± 1.1
	PLAc/Mg	32.6 ± 0.6	1.1 ± 1.5	0.02 ± 0.05	15.2 ± 2.0	33.6 ± 2.1
	PLAc/Qr/Mg	32.5 ± 1.1	2.6 ± 1.7	0.11 ± 0.12	15.6 ± 2.8	35.1 ± 2.8
	PLAa	31.9 ± 0.6	1.7 ± 0.6	0.04 ± 0.03	16.0 ± 1.3	33.6 ± 1.2
	PLAa/Qr	31.9 ± 1.0	1.7 ± 0.8	0.04 ± 0.04	16.0 ± 1.3	33.6 ± 1.8
	PLAa/Mg	33.7 ± 2.1	1.4 ± 1.4	0.04 ± 0.06	14.1 ± 4.7	35.1 ± 3.5
	PLAa/Qr/Mg	32.6 ± 0.7	2.3 ± 1.1	0.08 ± 0.07	14.9 ± 2.6	34.9 ± 1.8
Irradiated	PLAc + UV	30.2 ± 1.5	0.7 ± 2.7	0.004 ± 0.033	28.5 ± 3.2	30.9 ± 4.2
	PLAc/Qr + UV	31.7 ± 1.0	0.5 ± 1.9	0.002 ± 0.018	23.9 ± 6.1	32.2 ± 2.8
	PLAc/Mg + UV	30.3 ± 1.0	0.2 ± 1.0	0.0005 ± 0.0044	27.6 ± 3.1	30.5 ± 2.0
	PLAc/Qr/Mg + UV	31.2 ± 1.3	0.8 ± 3.1	0.006 ± 0.049	23.9 ± 6.6	32.0 ± 4.4
	PLAa + UV	34.5 ± 1.4	1.6 ± 2.5	0.023 ± 0.073	29.4 ± 4.1	32.8 ± 4.0
	PLAa/Qr + UV	31.9 ± 1.4	0.4 ± 2.0	0.002 ± 0.016	26.1 ± 2.4	32.3 ± 3.5
	PLAa/Mg + UV	31.5 ± 2.0	3.7 ± 1.9	0.14 ± 0.12	25.3 ± 3.1	35.2 ± 3.9
	PLAa/Qr/Mg + UV	29.8 ± 1.1	1.6 ± 2.1	0.024 ± 0.058	27.9 ± 3.6	31.4 ± 3.1

hydrophobicity with crystallinity degree and dopant content.

Not only water, but also θ_e and θ_d are not influenced by crystallinity and quercetin and Mg presence, within experimental uncertainty, before and after UV-C irradiation.

Comparing the contact angles before and after UV-C irradiation, the only liquid that undergoes significant changes is water: there is a mean drop of about 10 degrees for each dopant and crystallinity condition. Nonetheless, there is no significant difference between θ_w, θ_e and θ_d values regarding dopant effect after UV exposure.

Table 1 shows the values for the different components and parameters of surface free energy involved in van Oss model. All the samples have the same surface free energy, within the experimental uncertainty, and γ_S values are comprised between 31 and 35 mJ m^{-2}. γ^{LW} brings together the non-polar or dispersive contributions of the surface energy, while γ^{A-B} represents the polar ones. Comparing both components, in all cases, no matter the film composition and irradiation state, γ^{LW} is bigger than γ^{A-B} and none of them manifests any dependence on dopant presence and crystallinity degree before and after UV exposure. The important electron-donating character of all surfaces must also be emphasized, in contrast to their low electron-accepting capacity. This asymmetry between γ^{+} and γ^{-} becomes even more evident after irradiating the surfaces, where γ^{-} increases by 50–100 %, decreasing the parameter γ^{+} by more than an order of magnitude, compared to non-irradiated samples. This large drop in γ^{+}, reaching values approximately equal to zero, is responsible for the practically zero values in the γ^{A-B} component found after irradiation.

3.5. Chemical and thermal characterization

3.5.1. FTIR-DRIFT evaluation

Fourier-transform infrared spectroscopy (FTIR) was employed for determining possible interactions between the PLA matrix (amorphous and crystalline) and the active dopants, quercetin, and magnesium. FTIR measurements were performed before and after UV exposure. This technique is quite suitable for identifying functional groups involved in the interfacial interaction of the polymer matrix and the fillers and those implicated in the UV photo-oxidation process of the surface.

FTIR spectra of each dopant condition has been compared before and after UV irradiation (Fig. 8, for amorphous PLA films, and Fig. 9, for the crystalline ones). Therefore, with this comparison we can evaluate the effect of the ultraviolet ageing treatment in absorbance bands associated with PLA/dopants system. Firstly, it is necessary to identify the main absorbance bands corresponding to PLA matrix. Then, we will focus on the modifications in those absorbance bands or the appearance of some new due to the incorporation of quercetin and/or magnesium.

Peaks associated with the IR spectra of neat amorphous PLA can be observed in Fig. 9 (PLAa condition). The appearance of absorbance bands at 2999 and 2945 cm^{-1} indicates the asymmetrical and symmetrical stretching modes of —CH group. It is also possible to observe the most PLA characteristic band of the carbonyl (—C = O) group at 1787 cm^{-1}. Then, symmetrical and asymmetrical bending vibrations of —CH_3 can be found at 1469 and 1396 cm^{-1} and deformation mode of —CH at 1288 cm^{-1}. There are also some characteristic peaks at 1236, 1144, 1100 and 1051 cm^{-1} of symmetrical and asymmetrical —C—O—C stretching, —CO stretching and —OH bending, respectively. From 950 to 551 cm^{-1}, peaks from —CH_3 rocking modes, —C—COO and —C—C stretching, —C═O bending and amorphous phase can be detected. However, after UV irradiation of amorphous PLA films, some absorbance bands appear, and others increase their intensity. On the one hand, a broad peak centred at 3512 cm^{-1} corresponding to —OH stretching from different degradation products pop up after ultraviolet exposure.

Besides, from 1672 to 1647 cm^{-1} absorbance bands appear associated to —C═C stretching emerge after irradiation treatment. On the other hand, absorbance bands related to the asymmetrical and symmetrical stretching modes of —CH, the —C═O stretching, and 1400–900 cm^{-1} interval increase their intensity due to UV-C light disturbance.

Conversely, when quercetin is added to the amorphous PLA matrix (PLAa/Qr in Fig. 8) there is no significant variation from the neat PLA non-irradiated spectrum. And even more, there is also no change in PLAa/Qr spectrum after UV exposure. Therefore, the presence of quercetin in the matrix seems to avoid the consequences of UV irradiation seen in the previous case. Nevertheless, when magnesium particles are incorporated to the amorphous PLA matrix, there is an analogous behaviour, but with a different origin, to that of the irradiated PLAa

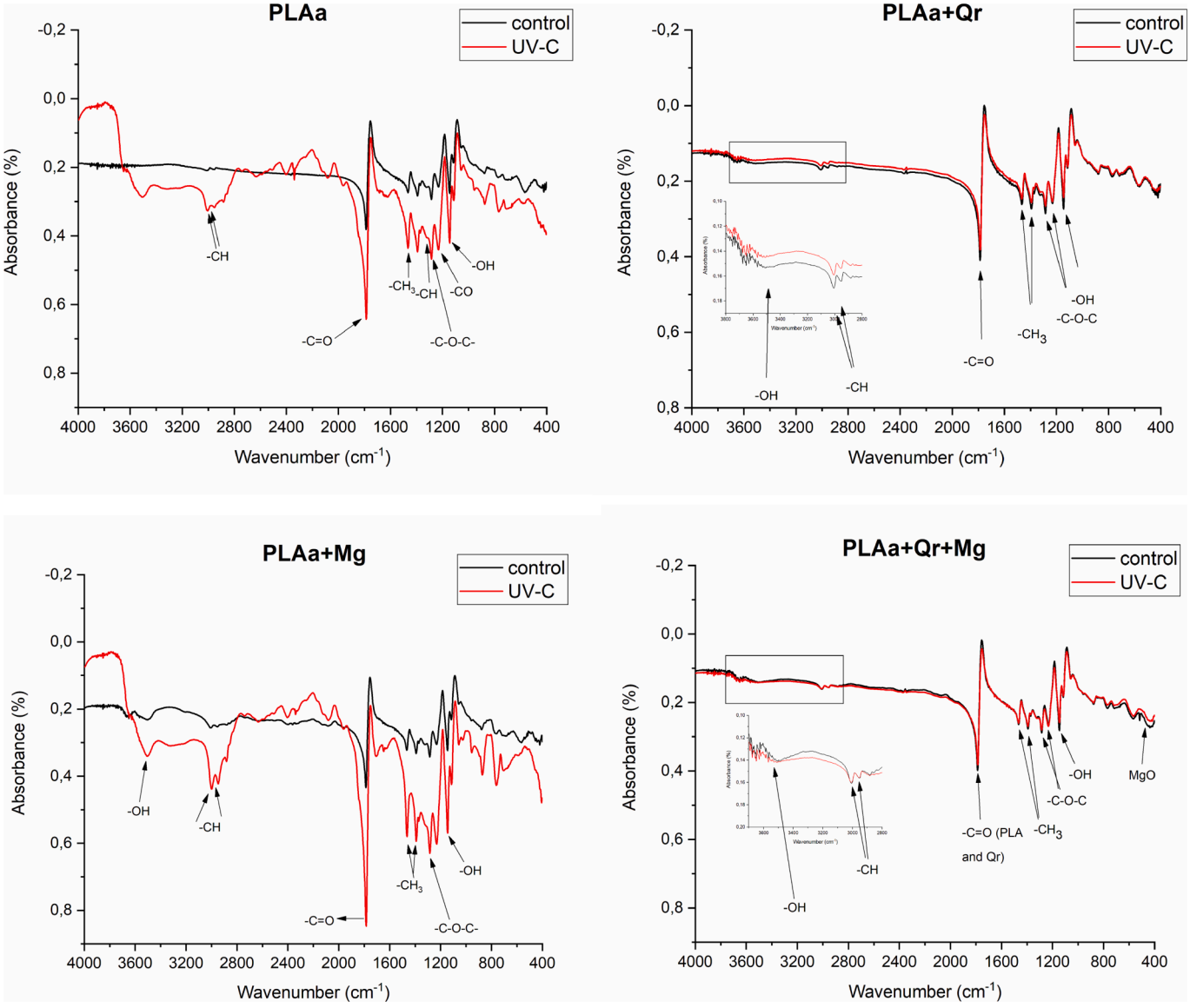

Fig. 8. FTIR spectra for amorphous PLA films in control (top left), quercetin (top right), magnesium (bottom left) and quercetin/magnesium (bottom right) conditions, before and after irradiation with UV-C light. In the graphics, "PLAa" stands for amorphous PLA films and "PLAc" for crystalline films.

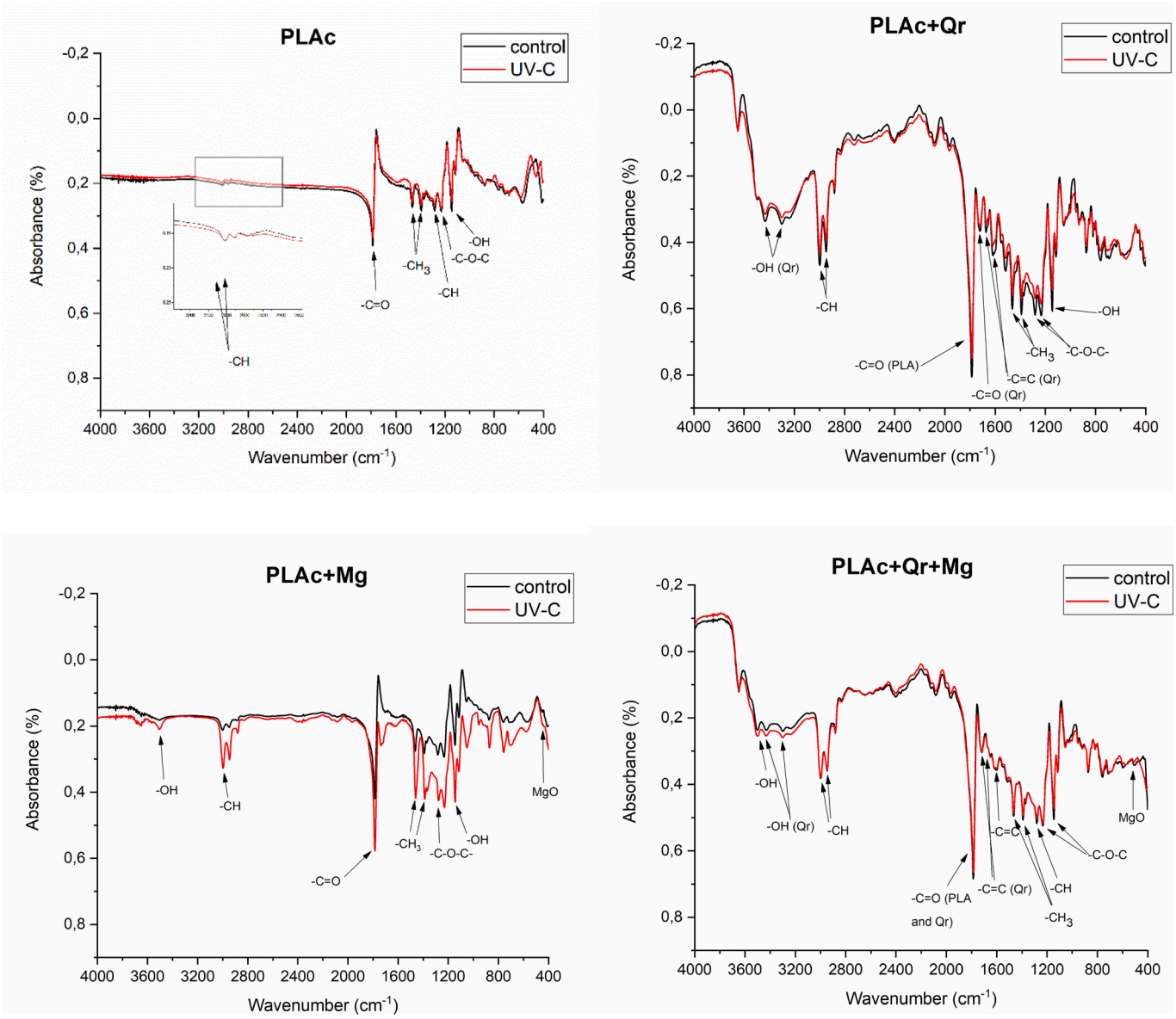

Fig. 9. FTIR spectra for crystalline PLA films in control (top left), quercetin (top right), magnesium (bottom left) and quercetin/magnesium (bottom right) conditions, before and after irradiation with UV-C light. In the graphics, "PLAa" stands for amorphous PLA films and "PLAc" for crystalline films.

Table 2
DSC parameters for amorphous and crystalline PLA films in control, quercetin, magnesium and quercetin + magnesium conditions before and after UV-C irradiation.

UV-C irradiation	Sample	DSC parameters				
		Tg (°C)	ΔC_p (J/g•K)	Melting area (J/g)	Tm (°C)	X_C (%)
Non-irradiated	PLAc manufacturer	59.5	0.307	31.27	149.52	33.6
	PLAc	59.5	0.335	23.89	151.02	25.7
	PLAc/Qr	61.8	0.209	25.43	150.52	27.3
	PLAc/Mg	56.6	0.277	23.51	151.25	25.3
	PLAc/Qr/Mg	60.6	0.307	23.29	150.01	25
	PLAa manufacturer	45.6	0.543	–		–
	PLAa	44.0	0.56	–		–
	PLAa/Qr	44.2	0.534	–		–
	PLAa/Mg	47.1	0.578	–		–
	PLAa/Qr/Mg	48.1	0.474	–		–
Irradiated	PLAc + UV	35.7	0.318	30	123.52	32.3
	PLAc/Qr + UV	42.7	0.304	28.7	146.02	30.9
	PLAc/Mg + UV	29.3	0.468	25.73	121.25	27.7
	PLAc/Qr/Mg + UV	44.2	0.291	28.28	148.51	30.4
	PLAa + UV	22.2	0.554	–		–
	PLAa/Qr + UV	41.5	0.424	–		–
	PLAa/Mg + UV	22.2	0.593	–		–
	PLAa + Qr-Mg + UV	43.2	0.502	–		–

condition. Absorbance bands from 3600 to 3200 cm^{-1} appear in the same way than for control amorphous PLA samples after irradiation but less intensified. The intensification of other absorbance bands already existing is repeated but they get more sharpened due to magnesium presence. Even more, when PLA/Mg composite is irradiated, some other absorbance bands appear, such as the 1693 and 1643 cm^{-1} from —C═C stretching, and the 455 cm^{-1} associated to MgO in our case. Thus, the comparison of the IR spectrum of PLAa/Mg condition with that of neat PLAa proves the incorporation of magnesium particles into the polymer matrix, and when the composite is exposed to UV-C light, the spectrum shows that the degradation process is even greater compared to the irradiated neat PLAa film. Interestingly, when quercetin and magnesium particles are both added to the PLA matrix, the non-irradiated spectrum remains unchanged compared to the control condition. Moreover, when UV treatment is applied, the PLAa/Qr/Mg spectrum does not show any modification. Thus, quercetin seems not only to avoid the consequences of ultraviolet exposure, but also seems to keep the PLA matrix away from magnesium presence effect, before and after UV disruption.

In the case of crystalline PLA films (Fig. 9), the non-irradiated neat PLA spectrum owns the same features than its amorphous analogous, except for the appearance of a specific band between 700 and 400 cm^{-1} ("fingerprint" zone). This may be related to the crystalline phase band. After UV irradiation, the control crystalline PLA spectrum stayed unaffected without suffering any remarkable modification.

The presence of quercetin in the polymer matrix is confirmed by examining the IR spectrum of the PLAc/Qr film. For instance, broad absorbance bands at 3431 and 3216 cm^{-1} are associated to hydroxyl groups in quercetin structure and absorbance bands at 1720, 1654 and 1618 cm^{-1} correspond to —C═O and —C═C (aromatic rings in quercetin) groups. Similar to the amorphous case, when magnesium particles are added to the crystalline PLA matrix before irradiation, there are some alterations compared to the PLAc control spectrum, due to the incorporation of these particles into the polymeric matrix. Furthermore, when PLAc/Mg sample is irradiated, the intensification of typical IR PLA absorbance bands and the appearance of some new others due to photo-oxidation process occur again. Nevertheless, in crystalline films that intensification is less pronounced than in amorphous ones, most probably related to crystallinity degree. Likewise, when quercetin and magnesium are both incorporated to the crystalline PLA matrix, the spectrum shows a very slight variation in the intensity of the absorbance bands respect to the unirradiated sample. Finally, to achieve a better comprehension about the effect of incorporation active fillers to an amorphous and crystalline PLA matrix, before and after UV irradiation, a representation of IR spectra of the different conditions has been provided in the Supplementary Material.

3.5.2. DSC analysis

The thermal response of different PLA films doped with quercetin and/or magnesium against UV-C irradiation was determined by using differential scanning calorimetry. The measurements were taken in closed aluminium pans under nitrogen atmosphere. DSC parameters T_g, T_m, and X_C, have been evaluated and depicted in Table 2. The melting temperature was taken as the peak of the melting endotherm. The glass transition temperature was taken as the inflection point of the specific heat decrement at the glass transition region. Consequently, the variation of specific heat at constant pressure, Δc_p, had to be calculated in that region. Moreover, X_C was calculated using the linear integration method, which evaluate the melting area under the DSC curve in the melting region.

In Fig. 10 DSC curves for amorphous PLA films with quercetin and/or magnesium before and after UV-C exposition have been plotted. DSC for amorphous PLA as provided by the manufacturer has also been included in the graphics. The most important information is that there is no melting zone, so there was not any crystalline phase to melt in these amorphous PLA films. It is only possible to discern a glass transition region. Despite that, visible changes can be appreciated regarding dopant presence and UV-C treatment. Before irradiation, there is no significant change in DSC curve after doping with quercetin and/or magnesium. However, after irradiation, PLAa and PLAa/Mg DSC curves suffered the most remarkable changes and glass transition temperature decrease considerably. Whilst those DSC curves corresponding to amorphous PLA films with quercetin remain practically unaltered after UV-C exposition. There is a clear decrease in their DSC peaks, but T_g does not largely change.

In Fig. 11, analogous DSC curves corresponding to crystalline PLA films can be appreciated. Also, crystalline PLA as received from the manufacturer has been included in this case. Comparing to amorphous films results, DSC curves for crystalline films with quercetin and/or

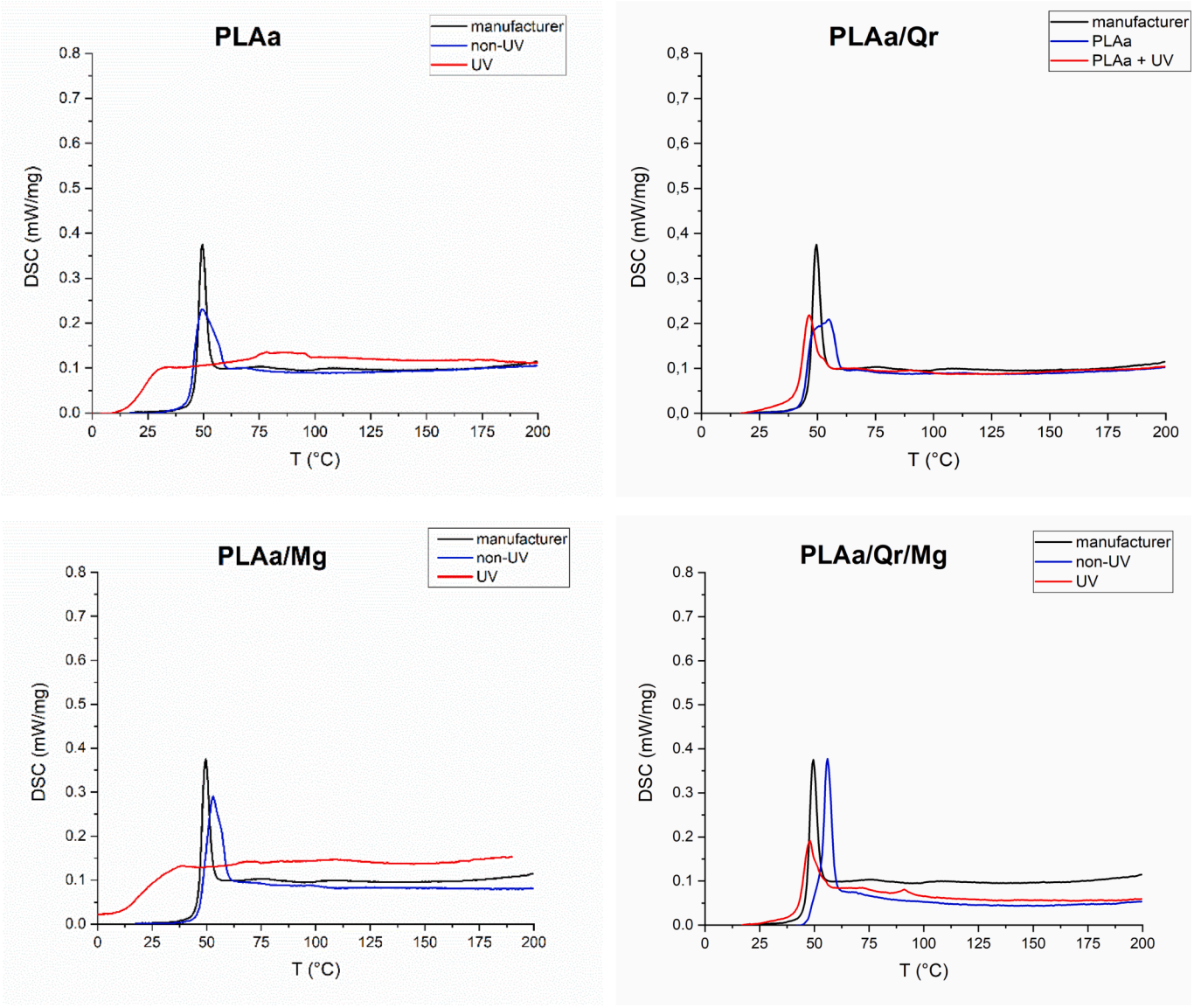

Fig. 10. DSC curves for amorphous PLA films in control (top left). Quercetin (top right). Magnesium (bottom left) and quercetin/magnesium (bottom right) conditions. Before and after irradiation with UV-C light. In the graphics. "PLAa" stands for amorphous PLA films and "PLAc" for crystalline films. Endothermic behaviour is set to upwards.

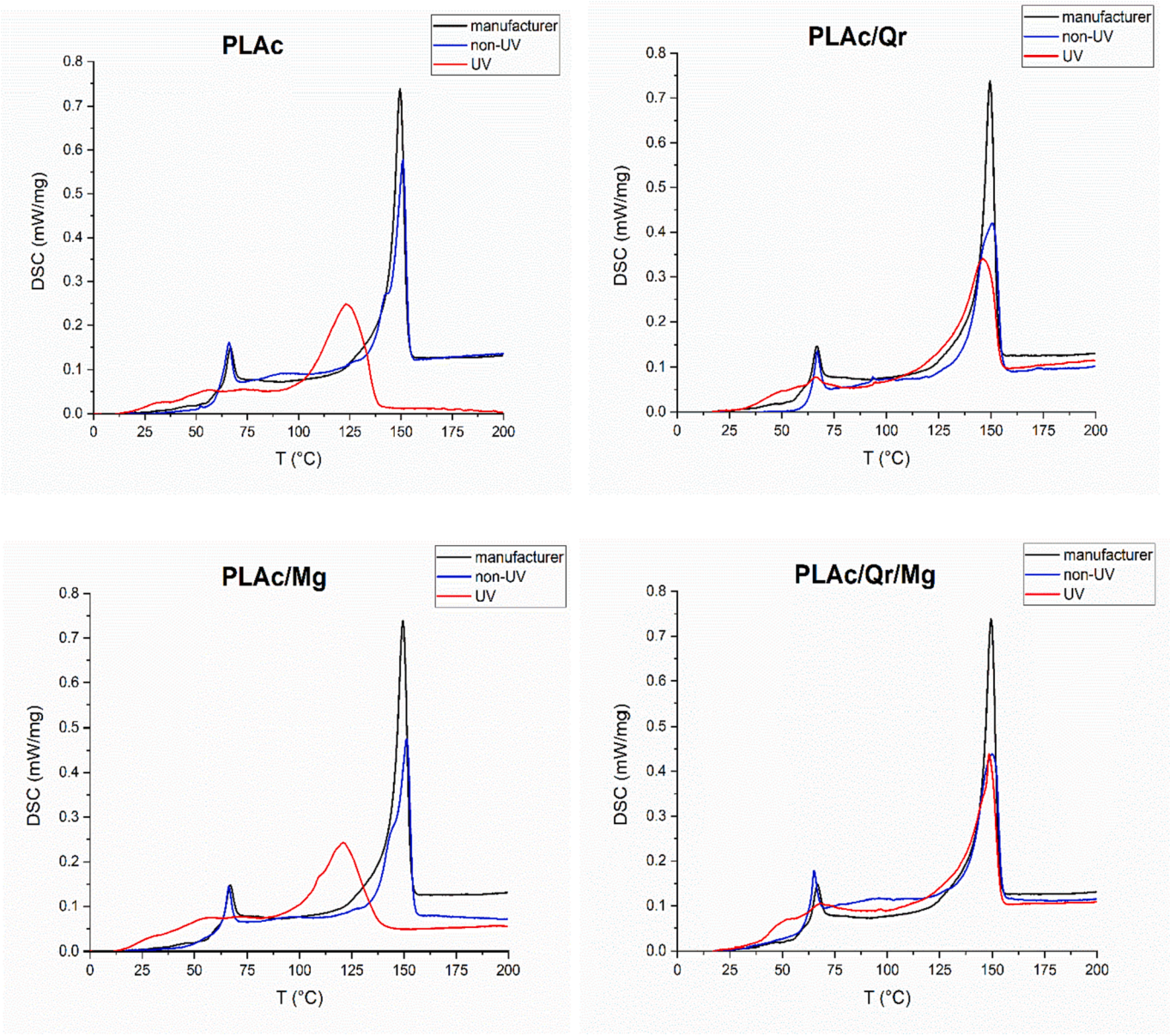

Fig. 11. DSC curves for crystalline PLA films in control (top left). Quercetin (top right). Magnesium (bottom left) and quercetin/magnesium (bottom right) conditions. Before and after irradiation with UV-C light. In the graphics. "PLAa" stands for amorphous PLA films and "PLAc" for crystalline films. Endothermic behaviour is set to upwards.

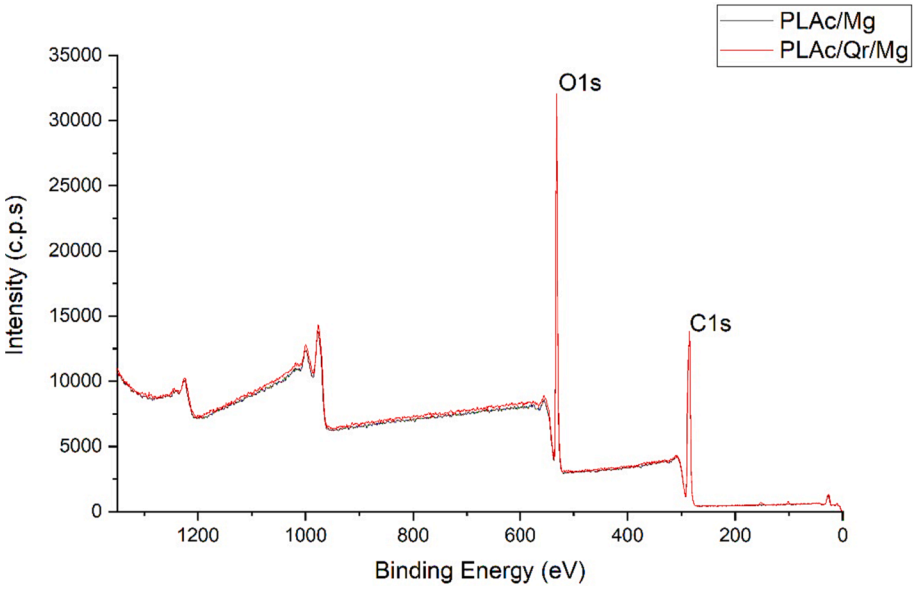

Fig. 12. Survey XPS spectra of crystalline PLA with Mg particles (PLAc/Mg) and with Mg particles and quercetin (PLAc/Qr/Mg).

Table 3
Relative atomic percentages obtained by XPS measurements on the surface of PLA films.

Crystallinity	Sample	Atomic Percentage [at%]			
		Non-irradiated		UV-C irradiated	
		C1s	O1s	C1s	O1s
Amorphous PLA	PLAa	63	37	63	37
	PLAa/Qr	66	33	64	36
	PLAa/Mg	63	37	63	35
	PLAa/Qr/Mg	63	35	63	35
Crystalline PLA	PLAc	63	37	63	36
	PLAc/Qr	63	37	61	37
	PLAc/Mg	63	37	64	36
	PLAc/Qr/Mg	63	36	62	37

magnesium before and after UV-C irradiation show a melting endotherm. Hence, this proves the existence of a crystalline phase in these films. Likewise, regarding the effect of dopant with UV treatment, before crystalline films were irradiated, DSC curves did not show important changes. However, once UV treatment was applied, the behaviour of DSC curves is quite similar to that from amorphous films. Only control crystalline films and those containing magnesium alone suffered the largest modifications, meanwhile those with quercetin remained close to the non-irradiated ones after UV exposure. In PLAa + UV and PLAa/Mg + UV, both T_g and T_m decreased respect to the non-irradiated values.

From Table 2, T_g values for amorphous films are lower in general than those from crystalline ones, as it could be expected for amorphous polymer. However, in both cases the glass transition temperature decreases after UV-C irradiation. Before UV treatment, Qr increases T_g in crystalline films meanwhile it does not have a specific effect in amorphous ones. But, after UV degradation, Qr maintains the glass transition temperature values similar to the non-irradiated ones, in both crystalline and amorphous cases. It occurs the same with T_m and X_C after ultraviolet exposure, Qr allows to maintain their values close to the non-irradiated crystalline films.

In the same way than FTIR results, other representations of DSC curves have been done and included in Supplementary Material (Figs. 4S and 5S). Those figures recover analogous information than Figs. 10 and 11 but from another point of view. They compare DSC curves regarding dopants incorporation in the same graphic, before and after UV-C irradiation, for both amorphous and crystalline cases.

3.5.3. XPS examination

XPS measurements were carried out to determine any conformational change in the outermost layers of the manufactured films. Fig. 12 shows, as a representative example, the survey spectra measured on the surface of two of the samples doped with magnesium particles. For all samples analysed, only carbon and oxygen are mostly detected on the surface, regardless of whether they contain magnesium particles (Table 3). Some elements such as silicon and nitrogen are detected on the surface of some of the samples analysed, but always in proportions below 1 %. Furthermore, no significant differences are observed in the percentages of elements detected on the surface of the different samples, irrespective of whether they have been subjected to UV-C treatment or not.

To verify if the presence of dopants or the treatment performed on the surface of the films affects the chemical environment of the elements detected by XPS, the high-resolution peaks are analyzed by performing a deconvolution. Due to the similar results obtained for every different condition, only those from PLAc/Mg and PLAc/Qr/Mg before and after UV treatment are implemented as an example. In all cases, the O1s peak is adjusted by three contributions attributed to the C—O, C═O and O—H bonds (Fig. 13). Considering the relationship between C—O/O—H bonds, an increase of O—H groups detected by deconvolution is observed on the surface of the samples which do not contain Mg particles when irradiated with UV-C light (Figs. 6S and 7S, provided in the Supplementary Material). However, this is not the case for amorphous PLA containing quercetin (PLAa/Qr), in which, after UV-C light treatment, a slight decrease in O—H bonds is observed (Fig. 7S). When magnesium is present in the films, the variations between the C—O/O—H ratio for untreated and treated samples are much reduced. A slight increase in the amount of O—H is observed for the PLAc/Qr/Mg + UV sample with respect to the non-irradiated one, whilst for the rest the

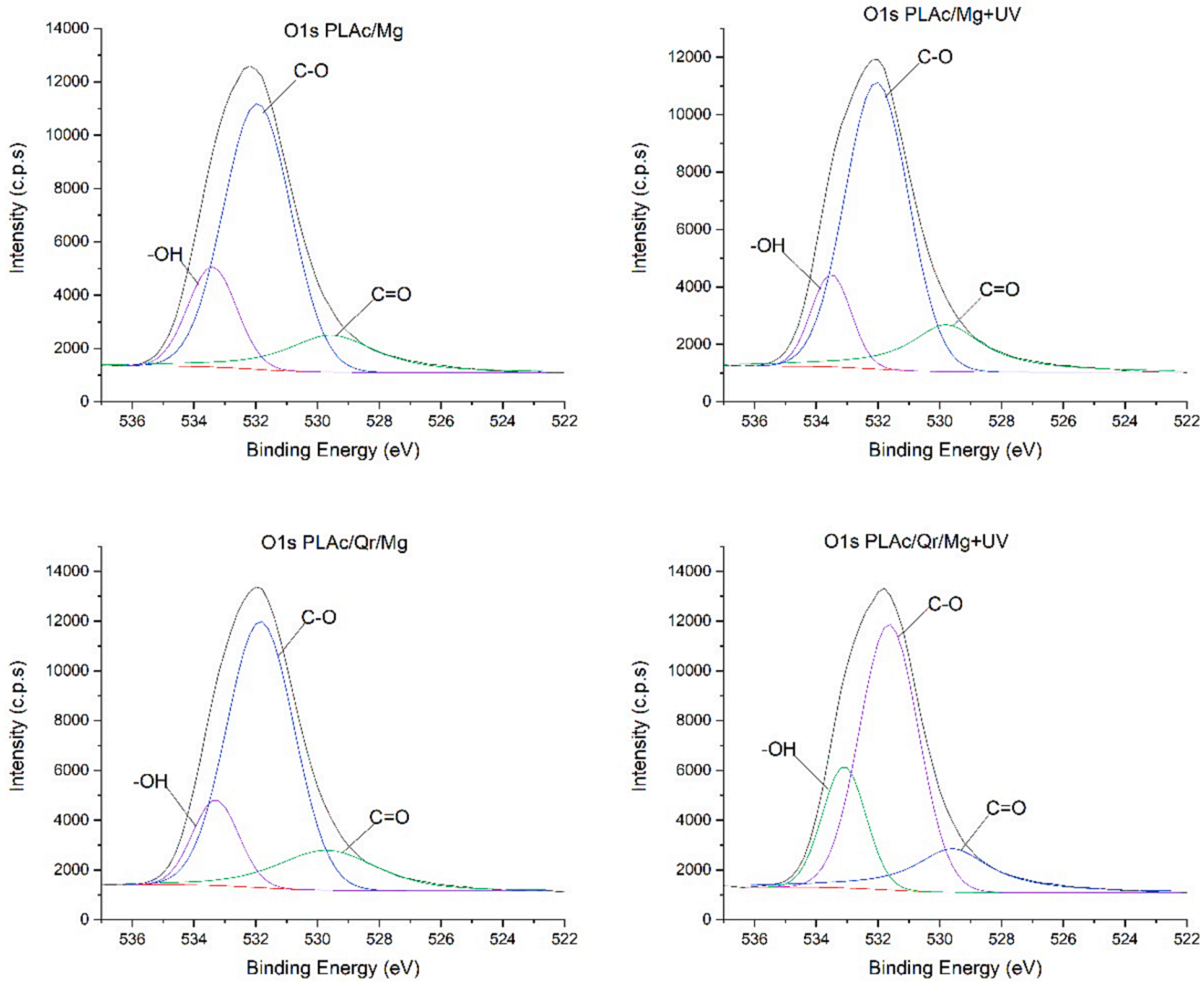

Fig. 13. High resolution O1s spectra of crystalline PLA films with Mg particles (PLAc/Mg) and with Mg particles and quercetin (PLAc/Qr/Mg), before and after UV light treatment.

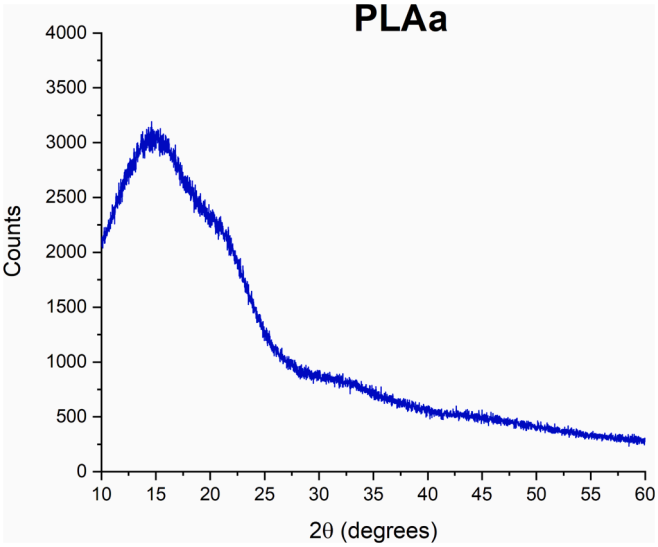

Fig. 14. XRD spectra of amorphous PLA film.

change detected in these bonds is not significant.

3.5.4. XRD evaluation

As it has been shown above in DSC results, PLAc partially adopts a crystalline structure after being dissolved in chloroform and cast on glass. To confirm these results, i.e., the existence of crystalline and amorphous structures in PLAc and PLAa, respectively, X-Ray diffractograms were recorded.

This test was performed in two replicates of each type of PLA (crystalline and amorphous) and in three different points of each replicate, in order to obtain consistent and robust statistics about the nature of the polymer structure in each film. However, only the first point of the first replicate have been incorporated to this work, shown in Figs. 14 (amorphous films) and 15(crystalline films). The diffractograms obtained are in well accordance with the DSC results previously described.

4. Discussion

The results presented in this work set the basis for discussing the physico-chemical benefits that the addition of active agents, such as quercetin and magnesium, can provide to PLA films when they face a degradation process by exposure to UV-C light. The extensive reviewed literature we have included in this work will allow us to use previous works to support our observations and/or hypotheses and shed light on the causes of the different results obtained by different authors when they have worked with polymer-ageing in conditions close to ours.

UV-C treatment introduced the most remarkable changes between samples in qualitative and quantitative data by all the techniques applied. From a **visual inspection**, the appearance of bubbles in PLAa + UV and PLAa/Mg + UV and the slight changes in the color of Qr-containing samples (Figs. 2 and 3) led to the hypothesis that some degradation/photooxidation process was happening under radiation, which caused the generation of different gases after chain scissions. This effect has just been observed by Wang et al. [79], who have proposed the formation of CO_2 and H_2O in PLA after excitation by ultraviolet exposure. In the case under study, the reduction in the number of bubbles in PLAa/Mg + UV, compared to PLAa + UV, means that Mg might reinforce the PLA matrix. In line with this result, the other dopant Qr is able to completely avoid the formation of bubbles inside this amorphous polymeric matrix. Not only the bubble reduction-elimination is a consequence of PLA doping but also of the degree of crystallinity. In this respect, we have found that a higher crystallinity degree prevents the formation of such structures probably due to a more efficient molecular packaging of the crystalline state and to the greater hydrogen-bonding interaction of certain groups, making it more resistant against degradation under ultraviolet exposure.

Analysis of the **IR spectra** of all prepared samples (Figs. 8 and 9) confirms the hypothesis that the bubbles observed in the films correspond to gases generated during the photooxidation of the films. Noticeable changes are mainly observed in the spectra of those samples showing bubbles after exposure to UV-C radiation, indicating a natural antioxidant effect of embedded quercetin in the PLA matrix and a higher stability of the crystalline lattice structure against UV-induced ageing

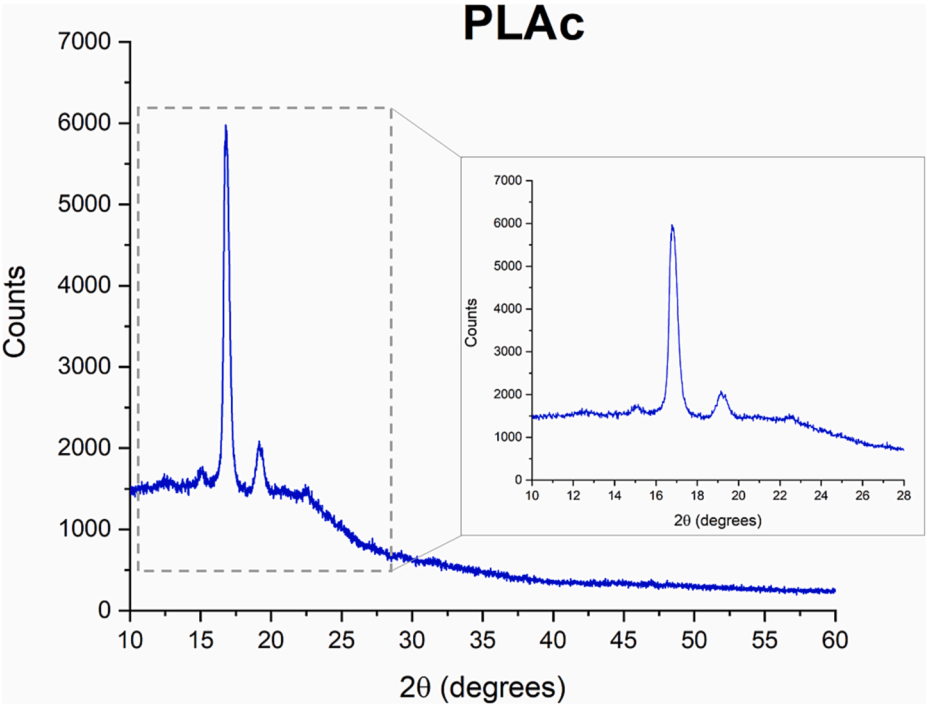

Fig. 15. XRD spectra of crystalline PLA film.

processes. In fact, Kun and Marossy [106] have already indicated that hydrolytic cleavage of the PLA chain occurs preferentially in the amorphous regions. Thus, before UV irradiation, the typical IR absorbance bands of pristine amorphous PLA were found, from the stretching modes of —CH group to the amorphous "fingerprint" zone, as other authors closely did in their works [14,18,19,27,104,107–109]. After UV irradiation, the new absorbance bands were detected at —OH stretching, more complex bonds and —C═C stretching specific zones and those related to stretching modes of —CH and —C═O were intensified. Wang et al. [79] and other authors [2,74,78,103,110] suggested the application of a mechanism based on Norrish II reactions to explain the PLA photodegradation. Even more, Gardette et al. [103] and Olewnik-Kruszkowska [2] emphasised the use of this kind of reactions to describe the photolysis of PLA chains by ultraviolet exposure for wavelengths values under 300 nm. As in our case (UV-C, 254 nm), they assured the photo-scission of the aliphatic ester group in PLA matrix and the formation of degradation products such as acetic anhydride. The presence of these species is evidenced by the appearance of absorbance bands at 1845 cm^{-1} and 1160 cm^{-1} [2,45,70,71,73,77,103,110].

Evaluating the role of matrix dopants in the photooxidation of polymer films, we found that the addition of magnesium particles to the PLA matrix produced a similar effect in both amorphous and crystalline IR spectra, although the effect in the case of the former was much more pronounced. Before UV irradiation, some absorbance bands from 3600 to 3200 cm^{-1} and from 2600 to 1950 cm^{-1} appeared when magnesium was present in both types of PLA, being more intense in PLAa than in PLAc. Other authors [36,38–41,111] reported similar results when they added Mg or MgO particles to a composite based on PLA. Certainly, previous works [23,31,32,36,38,40,41] stated that magnesium particles act as a catalyser in the PLA degradation, favouring water absorption into PLA matrix due to its high hydrophilic behaviour. Some of them [23,31,32,40], even proposed a simple mechanism were magnesium corrosion and PLA hydrolysis combine, resulting in a net effect which will determine the degradation of the entire composite. This effect could be appreciated in the amorphous and crystalline IR spectra shown (Figs. 8 and 9) where Mg alters the chemical behaviour of the composites after irradiation, enhancing their degradation. The PLA hydrolysis induced by Mg particles would be also accompanied by photooxidation, which, in turn, will be moderated by the Mg presence since Mg^{2+} cations would help to stabilize the charges and radicals generated during the degradation. This may be related to the lower number of bubbles observed in PLAa/Mg + UV, compared to PLAa + UV.

The incorporation of quercetin resulted in different IR spectra for PLAa and PLAc films. Before UV irradiation, PLAa/Qr and PLAa/Qr/Mg spectra remained unmodified compared to PLAa. Nevertheless, in the case of PLAc/Qr and PLAc/Qr/Mg spectra, some absorbance bands associated with the Qr in the IR spectrum appeared at 3431, 3296 and 3216 cm^{-1}, indicating the presence of —OH groups in Qr molecule and at 1720, 1654 and 1618 cm^{-1}, from the stretching vibrations of —C═O and —C═C in Qr structure. These results agreed with those previously obtained by other authors [48–51,65,67,68,112–114] and suggest that the interaction between quercetin and PLA is affected by the different spatial packaging of their polymer chains found in both crystalline lattices. This may result in different embedding depths of Qr in PLAa and PLAc films but, in any case, after UV irradiation, Qr causes the spectra of the different composites to remain unchanged no matter the crystallinity. Nonetheless, quercetin molecule also seems to be affected by UV-C light, as it can be observed in the non-irradiated/irradiated Qr spectrum (Fig. 3S, provided in the Supplementary Material). Thus, after Qr irradiation, an increase in the intensity of the absorbance bands at 3390 and 1009 (associated with the hydroxyl groups of its structure), 1655 (due to the carbonyl group), 1612 (double bonds of the aromatic rings) and 457 (—C—H bending) cm^{-1} is observed. Rosiak et al. [115] determined by chromatographic analysis that quercetin does not degrade by ionising radiation and suggested that the effect of this radiation may be the production of ROS and, in particular, of the superoxide radical anion. The generation of these species in turn causes changes in intra- and intermolecular hydrogen bonding, which would explain the increased intensity of the aforementioned absorbance bands. These small changes induced in the quercetin molecule by UV-C light put films containing this flavonoid among those with the highest chemical stability after irradiation. It is very likely that, if the polymer degradation takes place, Qr acts as a scavenger of the generated free radicals and/or reduce their formation. The radical mechanism of photodegradation of the polymer is interrupted via the transfer of a hydrogen atom, with the consequent formation of a quercetin radical. This unpaired electron is delocalised in different resonant structures, leading to an energetically stable and therefore non-reactive structure [116]. In this sense, Luzi et al. [117] and Olewnik-Kruszkowska et al. [48] suggested that quercetin might reinforce PLA matrix due to the intermolecular interactions between hydrophilic groups in polymer matrix and the polyhydroxyl groups of quercetin.

The **thermal response** of the PLA films to UV exposure, through DSC analysis, is given by the results in Figs. 10 and 11 and in Table 2 (and also in Supplementary Material in Figs. 4S and 5S). The neat PLA's DSC curve obtained before UV-C irradiation is quite similar to those previously obtained by Gardette et al. [103] or Chieng et al. [104] in their works. Particularly, the first ones obtained a T_g of 60 °C and a T_m of 149 °C, quite close to those obtained by us, as it is shown in Table 2. Also, films made with PLAa show lower T_g than those made with PLAc, which is logical since it is an amorphous polymer.

In the same way, after UV treatment, there is a clear drop of T_g for amorphous and crystalline films. T_m also decreased its values although it could only be appreciated for PLAc. This particular drop after exposing PLA to UV-C have also been reported by other authors such as Kosowska et al. [72], Visco et al. [76], Podzorova et al. [73] or Pinpathomrat et al. [70] for 4 h, 32 h, 100 h and 16 days of irradiation, respectively.

As it can be seen in both amorphous and crystalline cases, adding magnesium to the PLA matrix could not stop that drop in T_g and T_m values after UV-C irradiation. Indeed, in the case of crystalline films before UV treatment (Table 2), adding magnesium to PLA decreased T_g from 59.5 to 56.6 °C. This fact had also been observed by Antoniac et al. [111], when they doped PLA filaments with magnesium particles for 3D printing. They noticed that the presence of Mg induced the reduction in T_g assuming that interactions between filler particles and the polymer matrix reduced molecular mobility and flexibility of the chains in the filler surroundings.

Focusing on the degree of crystallinity, from the DSC information, of PLAc and PLAc/Mg films, both values are very similar, 25.7 % and 25.3 %, respectively. Furthermore, T_m values did not considerably change from PLAc to PLAc/Mg (from 151.02 to 151.25 °C). Following the argument exposed by several authors, such as Srivastava et al. [40] or Shuai et al. [32], one of the reasons that make magnesium particles act as nucleation agent is to increase T_m values. Particularly, Shuai et al. [32] stablished that the cause of Mg increasing the melting point might be associated to two alternative motives. First, Mg acted as a nucleation site and caused the crystallization to happen at higher temperatures, which leads to higher melting points. Second, Mg had a higher melting temperature than the polymer matrix and it would absorb some heat during the heating process, which allowed the polymer/filler composite melt at higher temperatures. And last but not least, in the case of our PLAa films, the inclusion of magnesium also did not induce any crystallinity. Hence, by these reasons, magnesium particles did not act as nucleating agents in the films prepared by the solvent-casting method followed in our case.

However, when Qr was added alone or together with magnesium, T_g and T_m maintained similar values to those from non-irradiated conditions. This is also the case of Czechowski et al. [3], where they irradiated for almost 16 h a PLA filament and stopped the drop in glass transition and melting temperatures by adding graphene nanoplatelets to the polymer matrix. And more relatable, Olewnik-Kruszkowska et al. [48] also observed an increment in T_g and T_m values as they increased the

amount of quercetin in a PLA/PEG blended system.

In summary, evaluating the DSC results, the tendency is quite similar to that obtained from FTIR. However, in this case it is also visible in crystalline films. After UV-C irradiation (Figs. 10 and 11), only those DSC curves with magnesium alone behave as the control ones after degradation. Nevertheless, when adding quercetin alone or with magnesium, the DSC curves after UV exposition behave similar to those from control conditions without being degraded by UV-C- light. Thus, quercetin allows to maintain the melting temperature in control values meanwhile magnesium makes it decrease after UV-C treatment. This might also be related to a degradation consequence that translates into thermal PLA behaviour and reinforces the idea of Qr as an antioxidant agent which rules the thermal response of PLA films against UV-C irradiation and overshadows the magnesium effect when added alone, in a very similar way as it could be observed in FTIR results.

The **crystallinity** of the PLA films comes to be reaffirmed with XRD results, which strongly supported those obtained from DSC analysis. In the same way that differential calorimetry did not record any melting endotherm (nor T_m value) in any of the PLAa films, i.e., any proof of crystalline phase existence, X-Ray diffractograms measured on two different PLAa (Fig. 14) films did not show any particular peak associated with crystalline structure either. This fact was already observed in previous works from our group [80]. In the case of PLAc films, a characteristic diffractogram of crystalline structure with identifiable peaks was observed (Fig. 15). In fact, those peaks were detected at $2\theta = 14.9°$, 16.8°, 19.3°, and 22.2°; characteristically found in the α crystalline phase. This result also agrees with those obtained by Luque-Agudo et al. [80], Rahman et al. [71] or Kaczmarek et al. [69]. Therefore, the existence of two clearly different crystallinities structures between PLAa and PLAc films has been qualitatively proved by XRD and quantified by DSC in this work.

The **hydrophobicity** of the PLA films before irradiation, by means of water contact angles, agrees with those obtained by other authors [25,38] and there are no changes regarding crystallinity degree, as other authors [118] have also pointed out, and regarding Qr and/or Mg inclusion. This result is in line with the idea of the existence of a thin layer of PLA in the outer surface under which dopants are embedded, as Hierro-Oliva et al. [119] have previously proved in their work. Similarly, He et al. [67] recorded no significant variation in θ_w values when they added MgO (20 % w/w) and quercetin (0.01, 0.1, 1 % w/w) to a PLGA fibred system. Ferrández-Montero et al. [28] also suggested the presence of an external PLA protective layer working with PLA-based composites. In any case, the manufacturing process of any polymer is crucial in its final hydrophobicity response due to the different orientation of the outer-most surface-exposed functional groups during the procedure, which is also affected by its internal structure conformation [81]. The effect of different preparation protocols can be underneath the different results found in bibliography when working with Qr or Mg. For instance, Masek et al. [120] reported an increase of 30.7 % in θ_w and 28.8 % in an epoxidized natural rubber system after loading Qr. Different works have indicated that the incorporation of magnesium particles increases the hydrophilic properties of the composite. Indeed, the θ_w values tend to decrease in presence of Mg due to the hydroxyl groups exposed on the surface of Mg particles (partly oxidised to magnesium oxide and hydroxide), increasing the probability of hydrogen-bonding with water. Besides, the available specific area of PLA/Mg composite is bigger compared to that of PLA matrix alone. In this line, there are authors who have shown changes after doping with quercetin and Mg. Other authors [20,38,121] have detected a reduction of the θ_w values as they increased the concentration of Mg particles inside the PLA/Mg composite.

After UV-C irradiation, there is a slight hydrophilization of all the surfaces, probably because of the photodegradation of that external PLA layer exposed to the environment. However, the hydrophobic hydrocarbon chains continue to be dominant in these degradation products, as suggested by Janorkar et al. [122]. Likewise, Visco et al. [76] also reported the decline of approximately 10 degrees in θ_w onto PLA after 32 h of UV-C photo-exposition, which is in line with the polarity increase already proposed by Rahman et al. [71].

The reduction in hydrophobicity of the samples has not significantly affected their surface free energy or components, but it has significantly increased the asymmetry in the electron-donor and electron-acceptor parameters, making γ^- much more important in the irradiated samples. This fact must be related to the surface radical activity of the polymer after irradiation and, in particular, to the generation of negative ionic species. It has already been demonstrated in a previous work from our group how the γ^- parameter is directly related to the negative zeta potential of the material [123], which is an indicator of the negative surface charge. Although in our work there is not any surface energy change after irradiation as consequence of the activation of the PLA boundary layer, other authors [107] have reported an increase in the total surface energy and its polar component when studying the solar ageing effect in an epoxidized natural rubber (ENR)/PLA blended system enriched with flavonoids. Probably, in that polymeric matrix, the exposition of flavonoids to the external surface of the material let them conclude that the antioxidant properties of these compounds slowed down the photooxidation process and the appearance of those excited functional groups.

The most important information extracted by **XPS** measurements is the confirmation of a thin polymeric layer above the dopant embedding zone due to the absence of quercetin and magnesium chemical "fingerprint", which support the information provided by goniometry analysis. This result also agrees with those presented by other authors [1,43], when detecting the presence of C═O bonds in the PLA matrix from O1s peak deconvolution. In particular, Chen et al. [124] detected a more intensified O1s peak, associated to pyran functional group in quercetin molecule, as the increased the Qr concentration in a PLLA scaffold. However, there is no trace of this specific peak in any of the samples analysed in our work (Figs. 13, S6 and S7). Moreover, the lack of detection of Mg on the surface of the Mg-containing samples (Fig. 12) by XPS indicates that Mg is also not found in the outermost layers of the films.

From the results obtained, it is very likely that the outermost surface activity of the films is different from the activity of the bulk after excitation. In the latter case, the presence of dopants, as well as the degree of crystallinity, influences the response of the material to ultraviolet radiation. For this reason, when characterizing a material with different techniques, it is very important to know from which part of the material the information is extracted. In the case of goniometry, the depth analyzed is between 3 and 20 Å and, as indicated above, corresponds to the outermost layer of the sample. X-ray photoelectron spectroscopy reaches depths between 10 and 250 Å and, in the case of FTIR, the ability of infrared radiation to penetrate into the matter means that this technique can reach depths of 1–5 μm, obtaining information from the material bulk [125].

In this sense, the indentation of the surface through a micrometer probe, such as an AFM tip, will allow to know the progressive tip-sample interaction from the outermost surface of the sample to a few microns in depth, drawing the mechanical behavior of the material surface and checking if it is affected by thermo-chemical and/or energetic properties obtained from FTIR, XPS, DSC, XRD and goniometry.

Young's modulus has shown an interplay between dopant presence, crystallinity degree and ultraviolet exposure. The mechanical response of PLA to dopants is not the same in crystalline and amorphous structures and so a different spatial distribution of the dopants regarding the crystallinity degree is expected, as previously stated. For amorphous, there is no significant changes in Young's modulus before and after quercetin and/or Mg addition, although the average values change in about 14 %. Nonetheless, when added to the crystalline films, quercetin and magnesium significatively decreased the Young's modulus of the matrix. Considering that IR has detected the presence of dopants a few microns from the surface of the crystalline matrix and that this zone

corresponds to the indentation depth of the tip, it is very likely that the decrease in Young's modulus is due to the mechanical weakening of the crystalline structure. This loss of mechanical properties is not so important in the amorphous matrix due to the more efficient integration of the dopants. Literature shows different mechanical responses of polymers to dopants. Olewnik-Kruszkowska et al. [48] or Latos-Brozio et al. [126] described an increase in elastic moduli when incorporated quercetin to PLA and PLA/poly(ethylene glycol) polymers. However, others, like Ezati et al. [68], have reported a decrease similar to that of this work of approximately 27 % after loading quercetin into PLA films. Likewise, the reduction in Young's modulus after magnesium particles bonded to the crystalline PLA matrix has also been communicated by other authors, such as Argentati et al. [38]. These authors investigated the effect of different concentrations of magnesium particles in the physical, chemical, and cell-viability properties of crystalline PLA films. In particular, for a 10 % (w/w) of magnesium particles, the same concentration used in this work, they recorded a drop of approximately 50 % in Young's modulus values for the PLA/Mg composite.

After UV-C ageing process, the tip-surface interaction was altered on both amorphous and crystalline PLA due to the significant drop in Young's modulus (E). Amza et al. [75], Zhao et al. [78] or Czechowski et al. [3] registered an approximately 2 %, 6 % and 25 % decrease of E after UV irradiation when analysing the changes in mechanical properties of 3D-printed elements based on PLA and PETG after 24 h of UV-C exposure and investigating the influence of nanoadditives in the UV ageing process of biopolymers by adding graphene nanopowder into printed PLA matrix. In our case, whilst dopants tended to decrease the Young's modulus of the composites when they were not exposed to ultraviolet light, once the samples were irradiated, the effect was just the opposite: the mechanical properties of the composites increased compared to the controls (Fig. 6).

There are several factors that influence the Young's modulus of the samples. One of them is the magnitude of the intermolecular interactions in the polymer chains. The smaller the interactions, the more elastic the material, and vice versa. Another factor, related to the intermolecular interactions, is the distance between the chains. The larger the distance, the smaller the intermolecular interactions and the more elastic the material.

UV-C irradiation must also be considered. UV-C light has opposing effects on Young's modulus. On the one hand, by inducing polymer degradation, its molecular mass decreases, thus increasing elasticity (E decreases). On the other hand, UV radiation, by breaking the covalent bonds of the polymer chain, can induce cross-linking of the polymer chains and thus increase their stiffness (increase in E). Moreover, it is found that the doped films show lower E than those that are not doped, as above mentioned. This higher elasticity may be due to the fact that, when the dopant molecules are introduced, the distance between the polymer chains increases and, therefore, the intensity of the intermolecular interactions decreases.

When the films are irradiated with UV-C light, E increases for doped films and decreases for non-doped films. In the latter case, the polymer degrades, the molecular weight decreases and, therefore, the elasticity increases. Besides, it has already been mentioned in this section that other authors registered a E loss in PLA systems, i.e., an increase of the elasticity, after UV exposition. For the former (doped films), although E increases, the cause is different. In PLAc/Mg films, where polymer degradation is notorious, charged species or high electron density are generated, which increases the intensity of intermolecular interactions. In PLA/Qr and PLA/Qr/Mg films, due to the protective effect of the Qr, the polymer is not degraded, but ROS are formed which alter the already existing intra- and intermolecular hydrogen bridge interactions, or new ones are produced, thus increasing the intensity of the intermolecular forces and, therefore, the Young's modulus.

The improvement (or preservation) of the mechanical properties of polymers by adding dopants is a topic of recent interest. In this sense, Stefaniak et al. [107] and Masek et al. [120] have studied the effect of adding different natural active compounds (vitamin E, curcumin, β-carotene and quercetin) in the ageing process of an ENR/PLA blended matrix, observing that quercetin was able to maintain the mechanical properties of the composite against UV ageing. Moreover, other authors, such as Czechowski et al. [3], increased the Young's modulus of a PLA matrix by designing a polymer-based composite with graphene-nanopowder particles after UV exposure. Probably, as shown in this work, the degree of crystallinity influences the magnitude of the observed changes, being the amorphous system the one that should better integrate the dopants in its structure and, consequently, alter more effectively its mechanical properties at the micrometer scale.

From a chemical point of view, the radical activity shown by the polymer after irradiation agrees with the lower Young's modulus of the control polymer compared to the irradiated ones (PLAa + UV < PLAa; PLAc + UV < PLAc). In this case, it is very likely that tip penetration into the material is favored by a tip-surface chemical interaction. However, as already mentioned, when dopants are present, after a first pristine activated polymeric matrix, the tip interacts with an excited composite where much of those radicals are scavenged by the dopants causing greater difficulty to indent the material. In any case, it should be noted that dopants do not always introduce a modification in the mechanical properties in the same direction, but it depends on other external factors such as exposition to UV radiation and, to a lesser extent, on internal factors such as the crystallinity of the material.

5. Conclusions

In the field of new composite materials for biomedical and industrial purposes, the combined action of inorganic magnesium particles and organic quercetin powder as active fillers in PLA matrices have proved a positive effect against UV-C photooxidation, being quercetin the main antioxidant component.

The response of PLA to UV radiation begins to be defined on the basis of its chains configuration: a crystallized lattice structure acts as a stronger barrier against UV-C light than an amorphous disposition. From a chemical point of view, amorphous PLA matrices show better integration of dopants than crystalline ones and, after UV-C irradiation, both structures enhance their mechanical properties when quercetin and/or Mg are present.

In PLA/Mg composites, degradation is enhanced by the catalytic effect of Mg, provoking the hydrolysis of the PLA chains. This effect is well appreciated in FTIR and DSC results.

Quercetin rules the chemical and thermal behaviour of the polymer against UV-C irradiation. Indeed, its presence in PLA/Qr/Mg samples prevents the degradation of the polymer, suppressing the catalytic process and protecting the polymer from chemical photooxidation. In addition, Qr improves the surface mechanical properties of the new biocomposite.

The benefits of the observed changes will be conditional on the specific application of the material in fields such as biomedicine, the food industry and other business sectors, where UV-C exposure is often unavoidable. Further advanced studies in this newly generated PLA/quercetin/magnesium composite degradation under other weathering processes are needed to broaden the perspectives of these materials in biomedicine and industry. In particular, microbial response against this composite surface and the complex chelation bonds of quercetin and magnesium are worthy of investigation.

CRediT authorship contribution statement

Juan M. Casares-López: Conceptualization, Data curation, Formal analysis, Methodology, Writing – original draft, Investigation. **Margarita Hierro-Oliva:** Conceptualization, Data curation, Formal analysis, Methodology, Supervision, Writing – original draft, Investigation. **Verónica Luque-Agudo:** Conceptualization, Data curation, Formal analysis, Investigation, Methodology, Supervision, Writing – original

draft. **M. Luisa González-Martín:** Writing – review & editing, Validation, Project administration, Resources, Supervision, Investigation, Methodology, Funding acquisition, Conceptualization. **Amparo M. Gallardo-Moreno:** Conceptualization, Funding acquisition, Investigation, Methodology, Project administration, Resources, Supervision, Validation, Visualization, Writing – review & editing.

Declaration of competing interest

The authors declare the following financial interests/personal relationships which may be considered as potential competing interests: Amparo M. Gallardo-Moreno reports financial support was provided by University of Extremadura. Amparo M. Gallardo Moreno reports financial support was provided by Spain Ministry of Science and Innovation. Amparo M. Gallardo-Moreno reports financial support was provided by Extremadura Government. Amparo M. Gallardo-Moreno reports financial support was provided by State Agency of Research. Amparo M. Gallardo-Moreno reports financial support was provided by European Regional Development Fund. Amparo M. Gallardo-Moreno reports a relationship with University of Extremadura that includes: employment.

Data availability

Data are contained within the article.

Acknowledgements

Authors are grateful to projects TED2021-131345B-I00, supported by MCIN/AEI/10.13039/501100011033/FEDER "Una manera de hacer Europa", IB20092 supported by Government of Extremadura and Project Action VI-03 supported by University of Extremadura, Spain. Contact angle and XPS measurements were performed by the ICTS "NANBIOSIS", more specifically by the Surface Characterization and Calorimetry Unit of the CIBER in Bioengineering, Biomaterials and Nanomedicine (CIBER-BBN) and the SACSS-SAIUEx of the University of Extremadura (UEx).

Appendix A. Supplementary material

Supplementary data to this article can be found online at https://doi.org/10.1016/j.apsusc.2023.159230.

References

[1] Y. Li, S. Qiu, J. Sun, Y. Ren, S. Wang, X. Wang, W. Wang, H. Li, B. Fei, X. Gu, S. Zhang, A new strategy to prepare fully bio-based poly(lactic acid) composite with high flame retardancy, UV resistance, and rapid degradation in soil, Chem. Eng. J. 428 (2022), https://doi.org/10.1016/j.cej.2021.131979.
[2] E. Olewnik-Kruszkowska, I. Koter, J. Skopińska-Wiśniewska, J. Richert, Degradation of polylactide composites under UV irradiation at 254 nm, J. Photochem. Photobiol. A Chem. 311 (2015) 144–153, https://doi.org/10.1016/j.jphotochem.2015.06.029.
[3] L. Czechowski, S. Kedziora, E. Museyibov, M. Schlienz, P. Szatkowski, M. Szatkowska, J. Gralewski, Influence of UV ageing on properties of printed PLA containing graphene nanopowder, Materials 15 (2022), https://doi.org/10.3390/ma15228135.
[4] M. Mizielińska, U. Kowalska, M. Jarosz, P. Sumińska, N. Landercy, E. Duquesne, The effect of UV aging on antimicrobial and mechanical properties of PLA films with incorporated zinc oxide nanoparticles, Int. J. Environ. Res. Public Health 15 (2018), https://doi.org/10.3390/ijerph15040794.
[5] A. Copinet, C. Bertrand, S. Govindin, V. Coma, Y. Couturier, Effects of ultraviolet light (315 nm), temperature and relative humidity on the degradation of polylactic acid plastic films, Chemosphere 55 (2004) 763–773, https://doi.org/10.1016/j.chemosphere.2003.11.038.
[6] N.P. Tipnis, D.J. Burgess, Sterilization of implantable polymer-based medical devices: a review, Int. J. Pharm. 544 (2018) 455–460, https://doi.org/10.1016/j.ijpharm.2017.12.003.
[7] P. Ezati, A. Khan, R. Priyadarshi, T. Bhattacharya, S.K. Tammina, J.W. Rhim, Biopolymer-based UV protection functional films for food packaging, Food Hydrocoll. 142 (2023), https://doi.org/10.1016/j.foodhyd.2023.108771.
[8] A.J.T. Teo, A. Mishra, I. Park, Y.J. Kim, W.T. Park, Y.J. Yoon, Polymeric biomaterials for medical implants and devices, ACS Biomater Sci. Eng. 2 (2016) 454–472, https://doi.org/10.1021/acsbioMaterials5b00429.
[9] E.E. García Carpintero, M. Cárdaba Arranz, L.M. Sánchez Gómez, Revisión bibliográfica sobre eficacia y seguridad de la luz ultravioleta y ozono para la desinfección de superficies. Actualización. Agencia de Evaluación de Tecnologías Sanitarias (AETS) - Instituto de Salud Carlos III, Ministerio de Sanidad. Madrid. Informes de Evaluación de Tecnologías Sanitarias, NIPO: 133-20-115-2, 2020.
[10] L.Y. Li, L.Y. Cui, R.C. Zeng, S.Q. Li, X.B. Chen, Y. Zheng, M.B. Kannan, Advances in functionalized polymer coatings on biodegradable magnesium alloys – a review, Acta Biomater. 79 (2018) 23–36, https://doi.org/10.1016/j.actbio.2018.08.030.
[11] L. Cai, D. Mei, Z.Q. Zhang, Y. Huang, L.Y. Cui, S.K. Guan, D.C. Chen, M. B. Kannan, Y. Zheng, R.C. Zeng, Advances in bioorganic molecules inspired degradation and surface modifications on Mg and its alloys, J. Magnesium Alloys 10 (2022) 670–688, https://doi.org/10.1016/j.jma.2022.02.005.
[12] R.G. Hu, S. Zhang, J.F. Bu, C.J. Lin, G.L. Song, Recent progress in corrosion protection of magnesium alloys by organic coatings, Prog. Org. Coat. 73 (2012) 129–141, https://doi.org/10.1016/j.porgcoat.2011.10.011.
[13] M. Nofar, D. Sacligil, P.J. Carreau, M.R. Kamal, M.C. Heuzey, Poly (lactic acid) blends: processing, properties and applications, Int. J. Biol. Macromol. 125 (2019) 307–360, https://doi.org/10.1016/j.ijbiomac.2018.12.002.
[14] R. Auras, B. Harte, S. Selke, An overview of polylactides as packaging materials, Macromol. Biosci. 4 (2004) 835–864, https://doi.org/10.1002/mabi.200400043.
[15] D.F. Williams, Biocompatibility: performance in the surgical reconstruction of man, Interdisc. Sci. Rev. 15 (1990) 20–33, https://doi.org/10.1179/isr.1990.15.1.20.
[16] K.F. Farraro, K.E. Kim, S.L.Y. Woo, J.R. Flowers, M.B. McCullough, Revolutionizing orthopaedic biomaterials: the potential of biodegradable and bioresorbable magnesium-based materials for functional tissue engineering, J. Biomech. 47 (2014) 1979–1986, https://doi.org/10.1016/j.jbiomech.2013.12.003.
[17] F. Witte, The history of biodegradable magnesium implants: a review, Acta Biomater. 6 (2010) 1680–1692, https://doi.org/10.1016/j.actbio.2010.02.028.
[18] S. Shankar, L.F. Wang, J.W. Rhim, Incorporation of zinc oxide nanoparticles improved the mechanical, water vapor barrier, UV-light barrier, and antibacterial properties of PLA-based nanocomposite films, Mater. Sci. Eng. C 93 (2018) 289–298, https://doi.org/10.1016/j.msec.2018.08.002.
[19] I. Kim, K. Viswanathan, G. Kasi, K. Sadeghi, S. Thanakkasaranee, J. Seo, Poly (lactic acid)/ZnO bionanocomposite films with positively charged ZnO as potential antimicrobial food packaging materials, Polymers (Basel) 11 (2019), https://doi.org/10.3390/polym11091427.
[20] D. Xu, Z. Xu, L. Cheng, X. Gao, J. Sun, L. Chen, Improvement of the mechanical properties and osteogenic activity of 3D-printed polylactic acid porous scaffolds by nano-hydroxyapatite and nano-magnesium oxide, Heliyon 8 (2022), https://doi.org/10.1016/j.Heliyon2022.e09748.
[21] A. John, K.P. Črešnar, D.N. Bikiaris, L.F. Zemljič, Colloidal solutions as advanced coatings for active packaging development: focus on PLA systems, Polymers (Basel) 15 (2023), https://doi.org/10.3390/polym15020273.
[22] E. Capuana, F. Lopresti, M. Ceraulo, V. La Carrubba, Poly-L-lactic acid (PLLA)-Based biomaterials for regenerative medicine: a review on processing and applications, Polymers (Basel) 14 (2022), https://doi.org/10.3390/polym14061153.
[23] S.C. Cifuentes, R. Gavilán, M. Lieblich, R. Benavente, J.L. González-Carrasco, In vitro degradation of biodegradable polylactic acid/magnesium composites: relevance of Mg particle shape, Acta Biomater. 32 (2016) 348–357, https://doi.org/10.1016/j.actbio.2015.12.037.
[24] P.B. Maurus, C.C. Kaeding, Bioabsorbable implant material review, Oper. Tech. Sports Med. 12 (2004) 158–160, https://doi.org/10.1053/j.otsm.2004.07.015.
[25] U. Boro, V.S. Moholkar, Antimicrobial bionanocomposites of poly(lactic acid)/ZnO deposited halloysite nanotubes for potential food packaging applications, Mater. Today Commun. 33 (2022), https://doi.org/10.1016/j.mtcomm.2022.104787.
[26] M. Drieskens, R. Peeters, J. Mullens, D. Franco, P.J. Iemstra, D.G. Hristova-Bogaerds, Structure versus properties relationship of poly(lactic acid). I. Effect of crystallinity on barrier properties, J. Polym. Sci. B: Polym. Phys. 47 (2009) 2247–2258, https://doi.org/10.1002/polb.21822.
[27] L.T. Sin, B.S. Tueen, Chemical properties of poly(lactic acid), in: Polylactic Acid, Elsevier, 2019, pp. 135–166, doi: 10.1016/b978-0-12-814472-5.00004-2.
[28] A. Ferrández-Montero, M. Lieblich, J.L. González-Carrasco, R. Benavente, V. Lorenzo, R. Detsch, A.R. Boccaccini, B. Ferrari, Development of biocompatible and fully bioabsorbable PLA/Mg films for tissue regeneration applications, Acta Biomater. 98 (2019) 114–124, https://doi.org/10.1016/j.actbio.2019.05.026.
[29] J. Stanley, A. John, K. Pušnik Črešnar, L. Fras Zemljič, D.A. Lambropoulou, D. N. Bikiaris, Active agents incorporated in polymeric substrates to enhance antibacterial and antioxidant properties in food packaging applications, Macromol. 3 (2022) 1–27, https://doi.org/10.3390/macromol3010001.
[30] C. Zhao, H. Wu, J. Ni, S. Zhang, X. Zhang, Development of PLA/Mg composite for orthopedic implant: tunable degradation and enhanced mineralization, Compos. Sci. Technol. 147 (2017) 8–15, https://doi.org/10.1016/j.compscitech.2017.04.037.
[31] X. Li, C. Chu, Y. Wei, C. Qi, J. Bai, C. Guo, F. Xue, P. Lin, P.K. Chu, In vitro degradation kinetics of pure PLA and Mg/PLA composite: effects of immersion temperature and compression stress, Acta Biomater. 48 (2017) 468–478, https://doi.org/10.1016/j.actbio.2016.11.001.

[32] C. Shuai, Y. Li, P. Feng, W. Guo, W. Yang, S. Peng, Positive feedback effects of Mg on the hydrolysis of poly-l-lactic acid (PLLA): promoted degradation of PLLA scaffolds, Polym. Test. 68 (2018) 27–33, https://doi.org/10.1016/j.polymertesting.2018.03.042.
[33] N. Sezer, Z. Evis, S.M. Kayhan, A. Tahmasebifar, M. Koç, Review of magnesium-based biomaterials and their applications, J. Magnesium Alloys 6 (2018) 23–43, https://doi.org/10.1016/j.jma.2018.02.003.
[34] X.N. Gu, S.S. Li, X.M. Li, Y.B. Fan, Magnesium based degradable biomaterials: a review, Front. Mater. Sci. 8 (2014) 200–218, https://doi.org/10.1007/s11706-014-0253-9.
[35] J. Rodríguez-Sánchez, M.Á. Pacha-Olivenza, M.L. González-Martín, Bactericidal effect of magnesium ions over planktonic and sessile *Staphylococcus epidermidis* and *Escherichia coli*, Mater. Chem. Phys. 221 (2019) 342–348, https://doi.org/10.1016/j.matchemphys.2018.09.050.
[36] A. Ferrández-Montero, A. Eguiluz, E. Vazquez, J.D. Guerrero, Z. Gonzalez, A. J. Sanchez-Herencia, B. Ferrari, Controlled SrR delivery by the incorporation of mg particles on biodegradable PLA-based composites, Polymers (Basel) 13 (2021), https://doi.org/10.3390/polym13071061.
[37] X. Yu, W. Huang, D. Zhao, K. Yang, L. Tan, X. Zhang, J. Li, M. Zhang, S. Zhang, T. Liu, B. Wu, M. Qu, R. Duan, Y. Yuan, Study of engineered low-modulus Mg/PLLA composites as potential orthopaedic implants: an in vitro and in vivo study, Colloids Surf. B Biointerfaces 174 (2019) 280–290, https://doi.org/10.1016/j.colsurfb.2018.10.054.
[38] C. Argentati, F. Dominici, F. Morena, M. Rallini, I. Tortorella, A. Ferrandez-Montero, R.M. Pellegrino, B. Ferrari, C. Emiliani, M. Lieblich, L. Torre, S. Martino, I. Armentano, Thermal treatment of magnesium particles in polylactic acid polymer films elicits the expression of osteogenic differentiation markers and lipidome profile remodeling in human adipose stem cells, Int. J. Biol. Macromol. 223 (2022) 684–701, https://doi.org/10.1016/j.ijbiomac.2022.11.005.
[39] A. Ferrández-Montero, M. Lieblich, R. Benavente, J.L. González-Carrasco, B. Ferrari, Study of the matrix-filler interface in PLA/Mg composites manufactured by Material Extrusion using a colloidal feedstock, Addit. Manuf. 33 (2020), https://doi.org/10.1016/j.addma.2020.101142.
[40] A. Srivastava, R. Ahuja, P. Bhati, S. Singh, P. Chauhan, P. Vashisth, A. Kumar, N. Bhatnagar, Fabrication and characterization of PLLA/Mg composite tube as the potential bioresorbable/biodegradable stent (BRS), Materialia (Oxf.) 10 (2020), https://doi.org/10.1016/j.mtla.2020.100661.
[41] N. Aničić, M. Kurtjak, S. Jeverica, D. Suvorov, M. Vukomanović, Antimicrobial polymeric composites with embedded nanotextured magnesium oxide, Polymers (Basel) 13 (2021), https://doi.org/10.3390/polym13132183.
[42] A. Anžlovar, A. Kržan, E. Žagar, Degradation of PLA/ZnO and PHBV/ZnO composites prepared by melt processing, Arab. J. Chem. 11 (2018) 343–352, https://doi.org/10.1016/j.arabjc.2017.07.001.
[43] Y. Huang, T. Wang, X. Zhao, X. Wang, L. Zhou, Y. Yang, F. Liao, Y. Ju, Poly(lactic acid)/graphene oxide-ZnO nanocomposite films with good mechanical, dynamic mechanical, anti-UV and antibacterial properties, J. Chem. Technol. Biotechnol. 90 (2015) 1677–1684, https://doi.org/10.1002/jctb.4476.
[44] É. da Cruz Faria, M.L. Dias, L.M. Ferreira, M.I.B. Tavares, Crystallization behavior of zinc oxide/poly(lactic acid) nanocomposites, J. Therm. Anal. Calorim. 146 (2021) 1483–1490, https://doi.org/10.1007/s10973-020-10166-3.
[45] A. Marra, S. Cimmino, C. Silvestre, Effect of TiO2 and ZnO on PLA degradation in various media, Adv. Mater. Sci. 2 (2017), https://doi.org/10.15761/ams.1000122.
[46] L.C. Mohr, A.P. Capelezzo, C.R.D.M. Baretta, M.A.P.M. Martins, M.A. Fiori, J.M. M. Mello, Titanium dioxide nanoparticles applied as ultraviolet radiation blocker in the polylactic acid bidegradable polymer, Polym. Test. 77 (2019), https://doi.org/10.1016/j.polymertesting.2019.04.014.
[47] H. Donya, R. Darwesh, M.K. Ahmed, Morphological features and mechanical properties of nanofibers scaffolds of polylactic acid modified with hydroxyapatite/CdSe for wound healing applications, Int. J. Biol. Macromol. 186 (2021) 897–908, https://doi.org/10.1016/j.ijbiomac.2021.07.073.
[48] E. Olewnik-Kruszkowska, M. Gierszewska, A. Richert, S. Grabska-Zielińska, A. Rudawska, M. Bouaziz, Antibacterial films based on polylactide with the addition of quercetin and poly(ethylene glycol), Materials 14 (2021), https://doi.org/10.3390/ma14071643.
[49] B. Parhi, D. Bharatiya, S.K. Swain, Application of quercetin flavonoid based hybrid nanocomposites: a review, Saudi Pharm. J. 28 (2020) 1719–1732, https://doi.org/10.1016/j.jsps.2020.10.017.
[50] N. Ghosh, T. Chakraborty, S. Mallick, S. Mana, D. Singha, B. Ghosh, S. Roy, Synthesis, characterization and study of antioxidant activity of quercetin-magnesium complex, Spectrochim. Acta A: Mol. Biomol. Spectrosc. 151 (2015) 807–813, https://doi.org/10.1016/j.saa.2015.07.050.
[51] N. Ghosh, R. Sandur, D. Ghosh, S. Roy, S. Janadri, Acute, 28 days sub acute and genotoxic profiling of Quercetin-Magnesium complex in Swiss albino mice, Biomed. Pharmacother. 86 (2017) 279–291, https://doi.org/10.1016/j.biopha.2016.12.015.
[52] T.S. de Castilho, T.B. Matias, K.P. Nicolini, J. Nicolini, Study of interaction between metal ions and quercetin, Food Sci. Human Wellness 7 (2018) 215–219, https://doi.org/10.1016/j.fshw.2018.08.001.
[53] C. Caro, M. Pourmadadi, M.M. Eshaghi, E. Rahmani, S. Shojaei, A.C. Paiva-Santos, A. Rahdar, R. Behzadmehr, M.L. García-Martín, A.M. Díez-Pascual, Nanomaterials loaded with Quercetin as an advanced tool for cancer treatment, J. Drug Deliv. Sci. Technol. 78 (2022), https://doi.org/10.1016/j.jddst.2022.103938.
[54] L. Wang, J. Dong, Z. Zhao, D. Li, W. Dong, Y. Lu, B. Jin, H. Li, Q. Liu, B. Deng, Quarternized chitosan/quercetin/polyacrylamide semi-interpenetrating network hydrogel with recoverability, toughness and antibacterial properties for wound healing, Int. J. Biol. Macromol. 228 (2023) 48–58, https://doi.org/10.1016/j.ijbiomac.2022.12.086.
[55] B. Kost, M. Svyntkivska, M. Brzeziński, T. Makowski, E. Piorkowska, K. Rajkowska, A. Kunicka-Styczyńska, T. Biela, PLA/β-CD-based fibres loaded with quercetin as potential antibacterial dressing materials, Colloids Surf. B Biointerfaces 190 (2020), https://doi.org/10.1016/j.colsurfb.2020.110949.
[56] D. Sun, N. Li, W. Zhang, E. Yang, Z. Mou, Z. Zhao, H. Liu, W. Wang, Quercetin-loaded PLGA nanoparticles: a highly effective antibacterial agent in vitro and anti-infection application in vivo, J. Nanopart. Res. 18 (2016) 1–21, https://doi.org/10.1007/s11051-015-3310-0.
[57] D. Sun, N. Li, W. Zhang, Z. Zhao, Z. Mou, D. Huang, J. Liu, W. Wang, Design of PLGA-functionalized quercetin nanoparticles for potential use in Alzheimer's disease, Colloids Surf. B Biointerfaces 148 (2016) 116–129, https://doi.org/10.1016/j.colsurfb.2016.08.052.
[58] M. Vinayak, A.K. Maurya, Quercetin loaded nanoparticles in targeting cancer: recent development, Anticancer Agents Med. Chem. 19 (2019) 1560–1576, https://doi.org/10.2174/1871520619666190705150214.
[59] A.M. Marchionatti, A. Pacciaroni, N.G. Tolosa de Talamoni, Effects of quercetin and menadione on intestinal calcium absorption and the underlying mechanisms, Comp. Biochem. Physiol. – Mol. Integr. Physiol. 164 (2013) 215–220, https://doi.org/10.1016/j.cbpa.2012.09.007.
[60] X. Cai, Z. Fang, J. Dou, A. Yu, G. Zhai, Bioavailability of quercetin: problems and promises, Curr. Med. Chem. 20 (2013) 2572–2582, https://doi.org/10.2174/09298673113209990120.
[61] P. Mukhopadhyay, A.K. Prajapati, Quercetin in anti-diabetic research and strategies for improved quercetin bioavailability using polymer-based carriers-a review, RSC Adv. 5 (2015) 97547–97562, https://doi.org/10.1039/c5ra18896b.
[62] M. Azeem, M. Hanif, K. Mahmood, N. Ameer, F.R.S. Chughtai, U. Abid, An insight into anticancer, antioxidant, antimicrobial, antidiabetic and anti-inflammatory effects of quercetin: a review, Polym. Bull. 80 (2023) 241–262, https://doi.org/10.1007/s00289-022-04091-8.
[63] M. Samsonowicz, E. Regulska, Spectroscopic study of molecular structure, antioxidant activity and biological effects of metal hydroxyflavonol complexes, Spectrochim. Acta A: Mol. Biomol. Spectrosc. 173 (2017) 757–771, https://doi.org/10.1016/j.saa.2016.10.031.
[64] M.M. Kasprzak, A. Erxleben, J. Ochocki, Properties and applications of flavonoid metal complexes, RSC Adv. 5 (2015) 45853–45877, https://doi.org/10.1039/c5ra05069c.
[65] F. Di Cristo, A. Valentino, I. De Luca, G. Peluso, I. Bonadies, A. Calarco, A. Di Salle, PLA nanofibers for microenvironmental-responsive quercetin release in local periodontal treatment, Molecules 27 (2022), https://doi.org/10.3390/molecules27072205.
[66] M.A. Sani, A. Dabbagh-Moghaddam, G. Jahed-Khaniki, A. Ehsani, A. Sharifan, A. Khezerlou, M. Tavassoli, M. Maleki, Biopolymers-based multifunctional nanocomposite active packaging material loaded with zinc oxide nanoparticles, quercetin and natamycin; development and characterization, J. Food Meas. Charact. (2023), https://doi.org/10.1007/s11694-022-01791-7.
[67] X. He, W. Liu, Y. Liu, K. Zhang, Y. Sun, P. Lei, Y. Hu, Nano artificial periosteum PLGA/MgO/Quercetin accelerates repair of bone defects through promoting osteogenic – angiogenic coupling effect via Wnt/ β-catenin pathway, Mater. Today Biol. 16 (2022), https://doi.org/10.1016/j.mtbio.2022.100348.
[68] P. Ezati, J.W. Rhim, Fabrication of quercetin-loaded biopolymer films as functional packaging materials, ACS Appl. Polym. Mater. 3 (2021) 2131–2137, https://doi.org/10.1021/acsapm.1c00177.
[69] H. Kaczmarek, M. Nowicki, I. Vuković-Kwiatkowska, S. Nowakowska, Crosslinked blends of poly(lactic acid) and polyacrylates: AFM, DSC and XRD studies, J. Polym. Res. 20 (2013), https://doi.org/10.1007/s10965-013-0091-y.
[70] B. Pinpathomrat, C. Narita, A. Yokoyama, K. Yamada, Evaluation of degradation of ultraviolet-C irradiated polylactic acid/carbon-fiber composites using fluorescence spectroscopy, Adv. Compos. Mater 31 (2022) 195–207, https://doi.org/10.1080/09243046.2021.1943108.
[71] M. Rahman, P. Opaprakasit, Effects of UV/photo-initiator treatments on enhancement of crystallinity of polylactide films and their physicochemical properties, J. Polym. Environ. 26 (2018) 2793–2802, https://doi.org/10.1007/s10924-017-1162-7.
[72] K. Kosowska, P. Szatkowski, Influence of ZnO, SiO2 and TiO2 on the aging process of PLA fibers produced by electrospinning method, J. Therm. Anal. Calorim. 140 (2020) 1769–1778, https://doi.org/10.1007/s10973-019-08890-6.
[73] M.V. Podzorova, Y.V. Tertyshnaya, P.V. Pantyukhov, A.A. Popov, S.G. Nikolaeva, Influence of ultraviolet on polylactide degradation, in: AIP Conf. Proc., American Institute of Physics Inc., 2017, doi: 10.1063/1.5013854.
[74] M.E. González-López, A.S. Martín del Campo, J.R. Robledo-Ortíz, M. Arellano, A. A. Pérez-Fonseca, Accelerated weathering of poly(lactic acid) and its biocomposites: a review, Polym. Degrad. Stab. 179 (2020), https://doi.org/10.1016/j.polymdegradstab.2020.109290.
[75] C.G. Amza, A. Zapciu, F. Baciu, M.I. Vasile, D. Popescu, Aging of 3d printed polymers under sterilizing UV-C radiation, Polymers (Basel) 13 (2021), https://doi.org/10.3390/polym13244467.
[76] A. Visco, C. Scolaro, H. Bellhamdi, A. Grasso, Photo-degradation of a biopolyester blend under UV-C rays, Macromol. Symp. 404 (2022), https://doi.org/10.1002/masy.202100330.
[77] B. Pinpathomrat, K. Yamada, A. Yokoyama, The effect of UV irradiation on polyamide 6/carbon-fiber composites based on three-dimensional printing, SN Appl. Sci. 2 (2020), https://doi.org/10.1007/s42452-020-03319-4.

[78] G. Zhao, M.R. Thompson, Z. Zhu, Effect of poly(2-ethyl-2-oxazoline) and UV irradiation on the melt rheology and mechanical properties of poly(lactic acid), J. Appl. Polym. Sci. 136 (2019), https://doi.org/10.1002/app.48023.

[79] Z. Wang, J. Ding, X. Song, L. Zheng, J. Huang, H. Zou, Z. Wang, Aging of poly (lactic acid)/poly (butylene adipate-co-terephthalate) blends under different conditions: environmental concerns on biodegradable plastic, Sci. Total Environ. 855 (2023), https://doi.org/10.1016/j.scitotenv.2022.158921.

[80] V. Luque-Agudo, A.M. Gallardo-Moreno, M.L. González-Martín, Influence of solvent and substrate on hydrophobicity of PLA films, Polymers (Basel) 13 (2021), https://doi.org/10.3390/polym13244289.

[81] V. Luque-Agudo, D. Romero-Guzmán, M. Fernández-Grajera, L. González-Martín, A.M. Gallardo-Moreno, Aging of solvent-casting PLA-Mg hydrophobic films: impact on bacterial adhesion and viability, Coatings 9 (2019), https://doi.org/10.3390/coatings9120814.

[82] V. Hasirci, N. Hasirci, Sterilization of Biomaterials, in: Fundamentals of Biomaterials, Springer New York, 2018, pp. 187–198, doi: 10.1007/978-1-4939-8856-3_13.

[83] Y.H. An, F.I. Alvi, Q. Kang, M. Laberge, M.J. Drews, J. Zhang, M.A. Matthews, C. R. Arciola, Effects of sterilization on implant mechanical property and biocompatibility, Int J Artif Organs 28 (11) (2005) 1126–1137, https://doi.org/10.1177/039139880502801110.

[84] Plastics, Methods of exposure to laboratory light sources. Part 3: Fluorescent UV lamps, CEN (European Committee for Standardization), 2016 (ISO 4892-3:2016).

[85] B. Pittenger, N. Erina, C. Su, Quantitative mechanical property mapping at the nanoscale with PeakForce QNM, Technical Report, Bruker (2010), https://doi.org/10.13140/RG.2.1.4463.8246.

[86] B. Cappella, G. Dietler, Surf. Sci. Rep. 34 (1999) 1–104, 0167-5729/99.

[87] L.M. Rebelo, J.S. De Sousa, J. Mendes Filho, M. Radmacher, Comparison of the viscoelastic properties of cells from different kidney cancer phenotypes measured with atomic force microscopy, Nanotechnology 24 (2013), https://doi.org/10.1088/0957-4484/24/5/055102.

[88] F. Rico, P. Roca-Cusachs, N. Gavara, R. Farré, M. Rotger, D. Navajas, Probing mechanical properties of living cells by atomic force microscopy with blunted pyramidal cantilever tips, Phys. Rev. E Stat. Nonlin. Soft Matter Phys. 72 (2005), https://doi.org/10.1103/PhysRevE.72.021914.

[89] G.G. Bilodeau, Regular Pyramid Punch Problem, J. Appl. Mech. 59 (1992) 519–523.

[90] R. Benítez, V.J. Bolós, J.-L. Toca-Herrera, afmToolkit: an R package for automated AFM force-distance curves analysis, R J. 9/2 (2017). ISSN 2073-4859.

[91] F. Rezgui, M. Swistek, J.M. Hiver, C. G'Sell, T. Sadoun, Deformation and damage upon stretching of degradable polymers (PLA and PCL), Polymer (Guildf.) 46 (2005) 7370–7385, https://doi.org/10.1016/j.polymer.2005.03.116.

[92] S. Farah, D.G. Anderson, R. Langer, Physical and mechanical properties of PLA, and their functions in widespread applications — a comprehensive review, Adv. Drug Deliv. Rev. 107 (2016) 367–392, https://doi.org/10.1016/j.addr.2016.06.012.

[93] S.M. Mirkhalaf, M. Fagerström, The mechanical behavior of polylactic acid (PLA) films: fabrication, experiments and modelling, Mech. Time Depend Mater. 25 (2021) 119–131, https://doi.org/10.1007/s11043-019-09429-w.

[94] S.C. Cifuentes, E. Frutos, R. Benavente, V. Lorenzo, J.L. González-Carrasco, Assessment of mechanical behavior of PLA composites reinforced with Mg microparticles through depth-sensing indentations analysis, J. Mech. Behav. Biomed. Mater. 65 (2017) 781–790, https://doi.org/10.1016/j.jmbbm.2016.09.013.

[95] X. Li, C.L. Chu, L. Liu, X.K. Liu, J. Bai, C. Guo, F. Xue, P.H. Lin, P.K. Chu, Biodegradable poly-lactic acid based-composite reinforced unidirectionally with high-strength magnesium alloy wires, Biomaterials 49 (2015) 135–144, https://doi.org/10.1016/j.bioMaterials2015.01.060.

[96] H. Mozafari, P. Dong, K. Ren, X. Han, L. Gu, Micromechanical analysis of bioresorbable PLLA/Mg composites coated with MgO: effects of particle weight fraction, particle/matrix interface bonding strength and interphase, Compos. B Eng. 162 (2019) 129–133, https://doi.org/10.1016/j.compositesb.2018.10.106.

[97] M.A. Pacha-Olivenza, A.M. Gallardo-Moreno, A. Méndez-Vilas, J.M. Bruque, J. L. González-Carrasco, M.L. González-Martín, Effect of UV irradiation on the surface Gibbs energy of Ti6Al4V and thermally oxidized Ti6Al4V, J. Colloid Interface Sci. 320 (2008) 117–124, https://doi.org/10.1016/j.jcis.2007.11.060.

[98] H.Y. Erbil, The debate on the dependence of apparent contact angles on drop contact area or three-phase contact line: a review, Surf. Sci. Rep. 69 (2014) 325–365, https://doi.org/10.1016/j.surfrep.2014.09.001.

[99] C.J. Van Oss, L. Ju, M.K. Chaudhury, R.J. Goodt, Estimation of the Polar Parameters of the Surface Tension of Liquids by Contact Angle Measurements on Gels, 1989, 0021-9797/89.

[100] C.J. Van Oss, R.J. Good, K. Chaudhury, Additive and Nonadditive Surface Tension Components and the Interpretation of Contact Angles, (1988) 0743-7463/88/2404-0884.

[101] C.J. Van Oss, M.K. Chaudhury, R.J. Good, Adv. Colloid Interface Sci. 28 (1987) 35–64, 0001-8686/87.

[102] J.W. Drelich, L. Boinovich, E. Chibowski, C. Della Volpe, L. Hołysz, A. Marmur, S. Siboni, Contact angles: history of over 200 years of open questions, Surf Innov. 8 (2020) 3–27, https://doi.org/10.1680/jsuin.19.00007.

[103] M. Gardette, S. Thérias, J.L. Gardette, M. Murariu, P. Dubois, Photooxidation of polylactide/calcium sulphate composites, Polym. Degrad. Stab. 96 (2011) 616–623, https://doi.org/10.1016/j.polymdegradstab.2010.12.023.

[104] B.W. Chieng, N.A. Ibrahim, W.M.Z.W. Yunus, M.Z. Hussein, Poly(lactic acid)/poly (ethylene glycol) polymer nanocomposites: effects of graphene nanoplatelets, Polymers (Basel) 6 (2014) 93–104, https://doi.org/10.3390/polym6010093.

[105] F. Di Cristo, A. Valentino, I. De Luca, G. Peluso, I. Bonadies, A. Di Salle, A. Calarco, Polylactic acid/poly(vinylpyrrolidone) co-electrospun fibrous membrane as a tunable quercetin delivery platform for diabetic wounds, Pharmaceutics 15 (2023) 805, https://doi.org/10.3390/pharmaceutics15030805.

[106] E. Kun, K. Marossy, Effect of crystallinity on PLA's microbiological behaviour, Mater. Sci. Forum 752 (2013) 241–247, https://doi.org/10.4028/www.scientific.net/MSF.752.241.

[107] K. Stefaniak, A. Masek, A. Jastrzębska, Biocomposites of epoxidized natural rubber modified with natural substances, Molecules 27 (2022), https://doi.org/10.3390/molecules27227877.

[108] V. Luque-Agudo, M. Hierro-Oliva, A.M. Gallardo-Moreno, M.L. González-Martín, Effect of plasma treatment on the surface properties of polylactic acid films, Polym. Test. 96 (2021), https://doi.org/10.1016/j.polymertesting.2021.107097.

[109] G. Kister, G. Cassanas, M. Vert, Effects of morphology, conformation and configuration on the IR and Raman spectra of various poly(lactic acid)s, 39(2) (1998) 267–273, S0032-3861(97)00229-2.

[110] S. Bocchini, K. Fukushima, A. Di Blasio, A. Fina, A. Frache, F. Geobaldo, Polylactic acid and polylactic acid-based nanocomposite photooxidation, Biomacromolecules 11 (2010) 2919–2926, https://doi.org/10.1021/bm1006773.

[111] I. Antoniac, D. Popescu, A. Zapciu, A. Antoniac, F. Miculescu, H. Moldovan, Magnesium filled polylactic acid (PLA) material for filament based 3D printing, Materials 12 (2019), https://doi.org/10.3390/ma12050719.

[112] A. Kumari, S.K. Yadav, Y.B. Pakade, B. Singh, S.C. Yadav, Development of biodegradable nanoparticles for delivery of quercetin, Colloids Surf. B Biointerfaces 80 (2010) 184–192, https://doi.org/10.1016/j.colsurfb.2010.06.002.

[113] A.M. Croitoru, Y. Karaçelebi, E. Saatcioglu, E. Altan, S. Ulag, H.K. Aydoğan, A. Sahin, L. Motelica, O. Oprea, B.M. Tihauan, R.C. Popescu, D. Savu, R. Trusca, D. Ficai, O. Gunduz, A. Ficai, Electrically triggered drug delivery from novel electrospun poly(lactic acid)/graphene oxide/quercetin fibrous scaffolds for wound dressing applications, Pharmaceutics 13 (2021), https://doi.org/10.3390/pharmaceutics13070957.

[114] S. Mathiyalagan, B.K. Mandal, Stability comparison of quercetin and its metal complexes and their biological activity, Biointerface Res. Appl. Chem. 11 (2021) 7890–7902, https://doi.org/10.33263/BRIAC111.78907902.

[115] N. Rosiak, J. Cielecka-Piontek, R. Skibiński, K. Lewandowska, W. Bednarski, P. Zalewski, Do rutin and quercetin retain their structure and radical scavenging activity after exposure to radiation? Molecules 28 (2023) 2713 https://doi.org/10.3390/molecules28062713.

[116] B. Cizmarova, B. Hubkova, A. Birkova, Quercetin as an effective antioxidant against superoxide radical, Funct. Food Sci. 3 (2023) 15, https://doi.org/10.31989/ffs.v3i3.1076.

[117] F. Luzi, E. Pannucci, L. Santi, J.M. Kenny, L. Torre, R. Bernini, D. Puglia, Gallic acid and quercetin as intelligent and active ingredients in poly(vinyl alcohol) films for food packaging, Polymers (Basel) 11 (2019), https://doi.org/10.3390/polym11121999.

[118] J. Li, Z. Li, L. Ye, X. Zhao, P. Coates, F. Caton-Rose, Structure and biocompatibility improvement mechanism of highly oriented poly(lactic acid) produced by solid die drawing, Eur. Polym. J. 97 (2017) 68–76, https://doi.org/10.1016/j.eurpolymj.2017.09.038.

[119] M. Hierro-Oliva, V. Luque-Agudo, A.M. Gallardo-Moreno, M.L. González-Martín, Characterization of magnesium-polylactic acid films casted on different substrates and doped with diverse amounts of ctab, Molecules 26 (2021), https://doi.org/10.3390/molecules26164811.

[120] A. Masek, S. Cichosz, Biocomposites of epoxidized natural rubber/poly(lactic acid) modified with natural substances: influence of biomolecules on the aging properties (part ii), Polymers (Basel) 13 (2021), https://doi.org/10.3390/polym13111677.

[121] C. Shuai, J. Zan, F. Qi, G. Wang, Z. Liu, Y. Yang, S. Peng, nMgO-incorporated PLLA bone scaffolds: enhanced crystallinity and neutralized acidic products, Mater. Des. 174 (2019), https://doi.org/10.1016/j.matdes.2019.107801.

[122] A.V. Janorkar, A.T. Metters, D.E. Hirt, Degradation of poly(L-lactide) films under ultraviolet-induced photografting and sterilization conditions, J. Appl. Polym. Sci. 106 (2007) 1042–1047, https://doi.org/10.1002/app.24692.

[123] A.M. Gallardo-Moreno, M.L. Navarro-Pérez, V. Vadillo-Rodríguez, J.M. Bruque, M.L. González-Martín, Insights into bacterial contact angles: difficulties in defining hydrophobicity and surface Gibbs energy, Colloids Surf. B Biointerfaces 88 (2011) 373–380, https://doi.org/10.1016/j.colsurfb.2011.07.016.

[124] S. Chen, L. Zhu, W. Wen, L. Lu, C. Zhou, B. Luo, Fabrication and evaluation of 3D printed poly(l-lactide) scaffold functionalized with quercetin-polydopamine for bone tissue engineering, ACS Biomater. Sci. Eng. 5 (2019) 2506–2518, https://doi.org/10.1021/acsbioMaterials9b00254.

[125] B.D. Ratner, A.S. Hoffman, F.J. Schoen, J.E. Lemons, Biomaterials Science, Elsevier, San Diego, California, USA, 2004.

[126] M. Latos-Brozio, A. Masek, Impregnation of poly(Lactic acid) with polyphenols of plant origin, Fibres and Textiles in Eastern, Europe 28 (2020) 15–20, https://doi.org/10.5604/01.3001.0013.7308.